INSULATION STRUCTURE AND COIL RELIABILITY*

H. Brechna and E. Oster
Stanford Linear Accelerator Center, Stanford University, Stanford, California

Abstract

Insulation voids due to impregnation and potting failure, and delamination of insulation due to magneto-mechanical and thermomechanical forces lead frequently to coil deficiencies such as corona, accelerated aging, electrical breakdown between conductors and adjacent pancakes, or flashover from coil to magnet core or structural parts.

The prevention and evaluation of cavities and the determination of their size and distribution over the coil is a formidable task. However, an approach to determine the stresses on the insulation and corona, ionization effects on the thermoset, and reduction of the corona threshold due to environmental influences is discussed. Methods of prevention, detection, and evaluation of cavities are given. A nondestructive coil test program to evaluate the soundness of insulation is proposed.

I. Introduction

As recently as a few years ago, silicone varnish dipped, glass taped, hollow square conductor coils were fabricated for a number of powerful electromagnets. This insulation technique is now considered inferior due to the lack of rigidity in the finished structure. The varnish was found to soften at moderate operational temperatures and interturn shorts appeared after approximately three years of operation. In other cases, such as a small bubble chamber magnet coil at CERN, which was insulated with B-staged glass-cloth epoxy, the coil failed after less than one year of operation due to water penetration into the insulation. Coils have failed due to excessive electro- and magneto-mechanical stresses, nonuniform heating, nonprofessional impregnation, or other causes too complex and numerous to be discussed in a paper of this scope.

The exciting magnet coil has to fulfill a number of functions: It must provide the appropriate number of ampere-turns, be able to withstand electromagnetic and mechanical forces, and not fatique over the magnet lifetime due to operational hazards in a radiation environment where moisture, chemical fumes, and dust may be present. The space for the location of the windings is generally limited, and compact coils with high current densities need extensive cooling and good insulation. Direct cooling is essential for powerful electromagnets. Hollow rectangular conductors like that shown in Fig. 1a, and direct cooled multi-stranded conductors (as in Fig. 1b), or edge-cooled coils for high power densities, are common.

The mechanical structure and the shape of the coils are important factors in the magnet. Two-dimensional coils for use in H-type magnets (Fig. 2) are easily obtained, but cannot be used for all magnet types, particularly when high fields in the gap are required. Three-dimensional coils, as shown in Fig. 3 for a Panofsky quadrupole, are by far more difficult to wind and insulate; they occupy less space than two-dimensional coils, but require high power density.

*Work supported by U.S. Atomic Energy Commission.

An ever-present requirement in all cases is that the coils be reliable, because any insulation failure means shutdown of the operation; replacement and repair are costly, and the interruption of an experiment is frustrating and cumbersome. The coil insulation in powerful electromagnets has to provide electrical and thermal insulation and must withstand extreme mechanical and thermal stresses. Even modern insulation used in high-energy laboratories may fatigue early and lead to an electric breakdown.

Due to the limited space for coils, the requirements on coil tolerances are high. However, tight tolerances may lead to expensive coils, and loose tolerances to uneven surfaces where high specific surface pressure can damage the insulation.

In recent years coil winding and insulation techniques have undergone considerable change. From early cotton tape wrapped around conductor and dipped into a varnish, the modern coils use high tensile glass fiber cloth and thermosetting structures with additional electrical insulation materials, such as mica and asbestos, with additives such as pigments and suitable fillers and wetting agents present.

Tests of the new winding and insulation must be more stringent, too. Nondestructive coil testing has not only to show that the coil insulation is presently sound, but also must provide evidence that the coil is reliable and can withstand all stresses common in powerful magnets.

The presence of voids, cavities, or fissures leads to the development of corona, pockets of corrosive gasses or, in the presence of water vapor, of corrosive liquids. The detection and elimination of any insulation deficiencies is one of the most important and difficult tasks of the magnet designer.

II. Insulation Structure

The majority of coils fabricated for high-energy electromagnets use glass filament cloth as structural material and reinforcement for the impregnant, and high temperature thermosettings combined with electrical insulations such as ground mica, asbestos, and polyester web. The glass fabric acts also as a spacer between adjacent conductors and provides structural rigidity to the coil when used as additional ground insulation. If epoxy is used as a binder in combination with glass fabrics, the coil structure is rigid and the insulation may rupture in internal transition areas between pancakes due to high shear stresses. In some cases a more flexible and rugged insulation, such as Mylar tape combined with adhesives, is preferred; however, the coils must be supported externally. In areas where insulations are exposed to high irradiation levels, the binder must be loaded with an inorganic filler, such as granulous alumina, to withstand ionization damage. To improve the mechanical properties of the insulation epoxy, functional materials such as glycidoxyl-propyl trimethoxy-silane (Z-6040), are added to the thermoset.[1] To provide long pot life to a thermoset, in order to use it for wet-winding techniques, three-component epoxies are preferred. Accelerators are

added to the catalyst in order to prolong the useful pot life of the epoxies. To provide slightly flexible structures, appropriate "flexibilizers" are added to the thermoset, even if this reduces the deflection temperature.

Generally, epoxies are preferred over silicones due to their higher mechanical strength and ease in handling. Table I shows general properties of glass fiber-reinforced thermosettings, widely used in coil insulation.

The glass fiber tapes applied around the cleaned and sandblasted conductor and the toroidal ground wrap around individual double pancakes are medium-or open-weave high tensile E or S glass.[2] The glass fiber must be heat cleaned in order to burn the oil starch used in manufacturing the filaments (to make it compatible with the thermoset) and chemically treated to restore part of its initial strength.

The introduction of the thermoset into the coil insulation structure is accomplished by one or a combination of the following methods:

a. Dip and Stack: The dry taped and wound coil is submerged into the liquid resin. To prevent the thermoset from drainage during curing, a shrinkable "sacrifice" tape is wrapped around the coil.

b. "B-Stage": Epoxy-impregnated, semicured glass tape is applied around the conductor and on ground insulation. During the cure cycle, external pressure must be applied to all coil surfaces to realize a monolithic structure and guarantee the coil dimensional tolerances.

c. Wet Lay Up: This method is used seldom in coil design, but is necessary in highly filled thermosets, where the viscosity of the thermoset exceeds several Poise and a uniform resin penetration into the glass fiber is doubtful by other means. In this case, thermosets with a long pot life of several days are employed and the use of an open-weave glass tape is necessary. Application of high vacuum prior to cure is recommended.

d. Vacuum Impregnation: This is the most reliable impregnation method, where excellent mechanical tolerances may be achieved, and different vacuum impregnation techniques, such as the closed mold method, open mold, and cocoon method, are widely used. The tape insulation must be dried thoroughly at temperatures of 110° C minimum, evacuated until a vacuum of less than 0.5 mm is reached, and then the thermoset introduced to the dry tape under vacuum. Often after the vacuum is broken, external pressure is applied to all coil surfaces to insure dimensional tolerances and to prevent excessive thermoset buildup. Coil, mold, and vacuum tank should be kept at impregnation temperature in order to keep the thermoset viscosity at a minimum and insure uniform wetting and penetration.

TABLE I

Physical Properties of Glass Cloth Reinforced Thermosettings

Property	Epoxy [a]	Silicone [b]
Tensile strength in warp direction ($kg \cdot cm^{-2}$)	4070	1500
Young's Modulus ($kg \cdot cm^{-2}$) [c]	1.95×10^5	1.8×10^5
Compression strength ($kg \cdot cm^{-2}$)	3500	1600
Flexural strength ($kg \cdot cm^{-2}$)	5900	2850
Specific gravity ($gr \cdot cm^{-3}$)	1.9	1.6
Specific heat ($Ws \cdot gr^{-1}\,{}^{o}C^{-1}$)	0.75	0.7
Thermal conductivity ($W \cdot cm^{-1}\,{}^{o}C^{-1}$)	6.5×10^{-3}	10^{-2}
Thermal expansion coefficient (${}^{o}C^{-1}$) [d]	$(1.3\text{-}1.7) \times 10^{-5}$	2.3×10^{-5}
Deflection temperature (Martens) (°C)	160	190
Dielectric strength (volt cm^{-1}) [e]	2.4×10^5	1.5×10^5
Shrinkage during cure (%)	0.15	0.12
Resin content by weight (%)	30	38
Water absorption (% weight) [f]	0.3-0.5	0.1-0.25

[a] Epoxy: Ciba 6005, Cat 906, acc. BDMA, wetting agent Z6040.

[b] Silicone: Dow Corning R-7521 and dicumyl peroxide.

[c] At 70° C.

[d] As comparison: Copper: $17.1 \times 10^{-6}\,{}^{o}C^{-1}$.

[e] 0.1-cm-thick insulation plates, Volan A-treated, medium-weave plain glass cloth.

[f] 10 days immersed in water 60° warm.

III. Stresses in Coil Insulation

A. Stresses Due to Electromagnetic Forces

A general two-dimensional coil configuration is illustrated in Fig. 4a. Any other shapes, cylindrical or rectangular, can be derived from it as special cases. We assume in the treatment below that the force distribution per unit length is uniform. However, the stresses due to electromagnetic forces can be calculated at any coil cross section from Maxwell's equations and applied to the stress calculation given below. Using Fig. 4b, representing the coil neutral axis, the moment at a point B is given by:[3]

$$M_B = \frac{p_m b^2}{2} - \frac{p_m}{2s}(I_x + I_y) \qquad (1)$$

or

$$M_B = \frac{p_m b^2}{2} - \frac{p_m}{2(a+b)+R(\pi-4)} \left\{ \frac{1}{3}\left[(a-R)^3 + (b-R)^3\right] + \frac{\pi}{2}R^3 + \frac{\pi}{2}R\left[a^2 + b^2 + 2R^2 - 2R(a+b)\right] + a^2(b-R) + b^2(a-R) + 2R^2(a+b-2R)\right\} \qquad (2)$$

and the moment at A:

$$M_A = M_B + p_m(a^2 - b^2) \qquad (3)$$

The shear force at any cross section is calculated from

$$Q(y) = \frac{dM}{dy} = \pm\, p_m \cdot y \qquad (4)$$

The shear stress at a cross section A is accordingly

$$\tau_{mean} = \frac{p_m \cdot y}{A} \qquad (5)$$

The maximum shear stress over the curved part of the coil is calculated from

$$\tau_{max} = p_m \cdot \left(\frac{\alpha^2}{\alpha^2 - 1}\right) \cdot \frac{a}{A} \qquad (a > b)$$

with the ratio of the outer to the inner radii

$$\alpha = \frac{R_o}{R_i}$$

For a spark chamber magnet with the dimensions

$$a = 3m \qquad b = 2m \qquad R = 0.5m$$

we get:

$$M_B = -\,1.876\, p_m$$

$$M_A = +\,3.124\, p_m$$

$$\tau_{mean} = p_m \cdot \frac{a}{A}$$

and for $R_o/R_i = 2$,

$$\tau_{max} = 4p_m/A$$

The pressure due to the electromagnetic forces can be calculated from the electromagnetic energy density per unit volume:

$$\frac{dW}{dV} = B \cdot H \qquad (6)$$

$$\frac{dW}{dV} = S \cdot A \qquad (7)$$

The magnetic stress in the cavity inside the coil is given by

$$p_m = \frac{B^2(x,y)}{2\,\mu_o} \qquad (8)$$

Assuming for the above spark chamber magnet a uniform field of $B = 2\ Wb/m^2$, the magnetic stress is

$$p_m = 16.244 \times 10^4\ kg\ m^{-2}$$

and:

$$M_B = 30.47 \times 10^4\ kg\ m$$

$$M_A = 50.74 \times 10^4\ kg\ m$$

with a maximum shear stress of

$$\tau_{max} = 199.93\ kg\ cm^{-2}\ \text{on the conductor},$$

and coil cross section

$$A = 0.325\ m^2$$

B. Equivalent Modulus of Elasticity

A coil is a composite structure of conductor material and insulation. The insulation thickness between adjacent layers is not negligible, and because of the bond between conductor and insulation, different expansion coefficients and shear, tensile, and compression stresses may act on the insulation. Assuming constant elongation per unit length, the forces on the coil may be written as

$$F = E\,(t_i \cdot E_i + t_c \cdot E_c) \qquad (9)$$

with the notations per unit length ($\ell \equiv 1$).

The stress per unit length is given by

$$\sigma = \frac{F}{t_i + t_c}$$

The equivalent modulus for tensile and compression E_{eq} is calculated in the classical theory form:

$$E_{eq} = \frac{1}{\sum_{\nu=1}^{n} t_\nu} \cdot \sum_{\nu=1}^{n} t_\nu\, E_\nu \qquad (10)$$

For a coil with:

$$t_c = 5\ cm \qquad t_i = 0.1\ cm$$

$$E_{Cu} = 1.25 \times 10^6\ (kg/cm^2)$$

$$E_{ins} = 7.5 \times 10^4\ (kg/cm^2)$$

$$E_{eq} = \frac{1}{5.1} \cdot (5.1 \times 1.25 \times 10^6 + 0.1 \times 7.5 \times 10^4)$$

$$\cong E_{Cu}$$

the classical theory yields too high values for the equivalent modulus. A relation which comes closer to experimental investigation is given in Eq. (11):

$$\frac{1}{E_{eq}} = \sum_{\nu=1}^{n} \frac{t_\nu}{E_\nu} \cdot \left(\frac{1}{t_\nu}\right) \qquad (11)$$

For the above case:

$$E_{eq} = 0.9562 \times 10^6 \ (kg/cm^2)$$

Using the equivalent modulus, we may treat the coil as a rigid entity with the modulus E_{eq} and calculate the stresses in the coil.

C. Mechanical Properties of the Insulation

The modulus of elasticity in tension and compression of glass fiber asbestos epoxy insulation varies with temperature, as shown in Fig. 5. The addition of asbestos insulation reduces the mechanical strength of the glass tape but is needed in many cases as electrical insulation, especially if B-staged or pre-impregnated glass tapes are used.

The Poisson ratio for the glass fiber-reinforced epoxy insulation is measured to be $\nu = 0.35$ and the modulus of elasticity in shear is

$$G = \frac{E}{2(1+\nu)} \qquad (12)$$

The ratio between shear and G is given by $\gamma = \tau/G$ and is normally small for glass-reinforced thermosets. The shear strength of glass fiber-reinforced epoxy (CIBA 6005, hardener 906 and accelerator 062) was measured after the following sample preparation: The hollow conductor was 20 cm long with a cross-sectional area of 5×5 cm, chemically cleaned and sandblasted. Insulation tapes used were glass fiber, Volan A-treated medium weave, 0.175 mm thick, 1 cm wide, half overlapped, and wrapped around the conductor three times. Three conductors were impregnated under 0.5-mm vacuum and, clamped in a press and cured for seven (7) hours at 180°C.

The test fixture is shown in Fig. 6.

The experimental values as an average of four samples are given in Table II. The shear strength was obtained after shearing the insulation and evaluating the actual bonded surface between conductors. In most cases more than 50% of the surface area between conductors was bonded. Holidays and unbonded spots were scattered randomly.

TABLE II

Shear Strength as Function of Temperature

Applied Temperature	Shear Strength
22°C	1.6×10^2 kg/cm^2
60°C	1.2×10^2 kg/cm^2
90°C	0.97×10^2 kg/cm^2

The tests on straight samples were repeated on a pancake shown in Fig. 7. The shear strength of straight sections was reduced by 13.6% and on curved sections by 8.4% lower than given in Table II.

D. Electrical Properties of the Insulation

The magnet insulation may be subject to dry or wet environmental conditions. It is known that glass-reinforced thermosets have great affinity toward water absorption.[4] The presence of moisture on glass epoxy surfaces leads to a surface corrosion process and the acceleration of fatigue properties. The effect of surface corrosion is enhanced in B-stage tapes, where moisture could be trapped in the glass filament matrix. Vacuum drying and vacuum impregnation is far superior and reduces moisture penetration markedly. The epoxy content in the filament matrix must be guarded carefully. In resin-rich insulation the moisture absorbtion may be reduced; however, the mechanical property of the insulation, as well as the tendency of epoxy to shrink during the curing process, may lead to local cracking or randomly distributed cavities. Resin-poor insulations have low bond strength and great affinity toward moisture absorption. As optimum values, about 18-23% parts of epoxy compound per weight of the total insulation can be recommended. The two types of insulation discussed in Section II need additional surface-protecting coatings to prevent the water from penetrating into the coil and reducing its dielectric strength. For our experimental setup the ground insulation was chosen to be mica-glass-fiber epoxy with an additional layer of 0.05 cm polyester-web impregnated in the same operation as the rest of the coil. The insulation between conductors was medium-weave, (Volan A-treated), glass cloth, and asbestos with an insulation thickness between adjacent conductors of approximately 0.1 cm.

The dielectric breakdown between conductors was 7.5 kV ± 20% and from conductor to ground (0.2 mm) about 20 kV ± 7% in dry conditions. Between adjacent conductors, the dielectric breakdown was 4.8 kV ± 9.5% after 94 hours immersion in tap water and 2.1 kV ± 30% after 300 hours in tap water, with an insulation resistance at 500 volts of better than 5×10^4 Mohms.

E. Shear Stresses in the Conductor Due to Thermal Gradients

For the coil configuration shown in Fig. 8, with a water inlet temperature T_i and the temperature gradient ΔT over the hydraulic passage, the mean temperature over a double pancake with N turns in series is expressed as

$$T_{mi} = T_{in} + \frac{\Delta T}{2}\left(1 - \frac{1}{N}\right) \qquad (13)$$

In this calculation we neglect the heat leak between inlet and outlet adjacent turns, which may lead to a parabolic temperature distribution over a hydraulic passage instead of a linear distribution.[5] By using approximately 0.1-cm-thick insulation between adjacent turns, the parallel heat path from hot to cold conductors is insignificant and does not affect the calculations given here.

The shear stress in the curved part of the coil is given by

$$\tau = \alpha E_c \cdot \Delta T \cdot h \cdot r^{-1} \qquad (14)$$

With the numbers

α = thermal expansion coefficient of copper = $17.\,10^{-6}\ ^{o}C^{-1}$

$$E_c = 1.25 \cdot 10^6 \text{ kg cm}^{-2}$$

$$\Delta T = 60^{o}C$$

the maximum shear stress on the conductor is:

$$\tau_{max} = 127.50 \text{ kg cm}^{-2}$$

and inside the conductor,

$$\tau_{max,\,max} = 191.5 \text{ kg cm}^{-2}$$

On the straight sections,[6]

$$\tau = \frac{2}{9} \cdot \alpha E \cdot \Delta T \cdot h \cdot \ell^{-1} \tag{15}$$

or calculated for our case,

$$\tau = 14.2 \text{ kg cm}^{-2}$$

The compressive stress in the curved parts between adjacent turns can be calculated using the relation:

$$\sigma_c = \alpha E \cdot (T_c - T_{mi}) \cdot b \cdot r^{-1} \tag{16}$$

and is illustrated for the coil considered in Fig. 8.

F. Mechanical Stress Distribution in the Insulation

With the stresses calculated in Eq. (5) in the copper conductor, the boundary stress values on the inner and outer insulation surfaces are known. The insulation is laminated and may delaminate under conditions of shear stress higher than bond strength. The calculations of the stress distribution for the curved parts are given below.

The stress distribution in an element shown in Fig. 4c is in general form:

$$\sigma_r \cdot r d\phi + \sigma_t \cdot dr d\phi - \left(\sigma_r + \frac{d\sigma_r}{dr} dr\right)(r + dr)d\phi = 0 \tag{17}$$

Neglecting higher-order terms, for a small angle $d\phi$ we get:

$$\frac{d\sigma_r}{dr} = \frac{\sigma_r - \sigma_r}{r} \tag{18}$$

With the relations:

$$\nu_{rt} \cdot E_t = \nu_{tr} \cdot E_r$$

(ν = Poisson's Ratio) and

$$k = \left(\frac{E_t}{E_r}\right)^{\frac{1}{2}}$$

we obtain the equations for elongation:

$$\epsilon_r = \frac{\sigma_r}{E_r} - \frac{\sigma_t}{\nu_{rt} \cdot E_t} = \frac{1}{E_r}\left(\sigma_r - \frac{1}{\nu \cdot k^2}\right)\sigma_t$$

$$\epsilon_t = \frac{\sigma_t}{E_r} - \frac{\sigma_r}{\mu E_t} = \frac{1}{k^2 E_r}\left(\sigma_t - \frac{1}{\nu}\,\sigma_r\right) \tag{19}$$

and the main stresses

$$\sigma_r = \frac{k^2\nu^2}{k^2\nu^2 - 1} \cdot E_r\left(\epsilon_r + \frac{1}{\nu}\,\epsilon_t\right)$$

$$\sigma_t = \frac{k^2\nu^2}{k^2\nu^2 - 1} \cdot E_r\left(\frac{1}{\nu}\,\epsilon_r + k^2\epsilon_t\right) \tag{20}$$

Introducing the displacement u at r and $u + \frac{du}{dr} dr$ at the radius r + dr, the per unit length elongation, we get:

$$\epsilon_r = \frac{du}{dr}$$

$$\epsilon_t = \frac{u}{r}$$

The stress equations can be modified to be

$$\sigma_r = \frac{k^2\nu^2}{k^2\nu^2 - 1} \cdot E_r\left(\frac{du}{dr} + \frac{1}{\nu}\,\frac{u}{r}\right)$$

$$\sigma_t = \frac{k^2\nu^2}{k^2\nu^2 - 1} \cdot E_r\left(\frac{1}{\nu} \cdot \frac{du}{dr} + k^2 \cdot \frac{u}{r}\right) \tag{21}$$

Substituting Eq. (21) into Eq. (18), we obtain the equation

$$\frac{d^2u}{dr^2} + \frac{1}{r}\frac{du}{dr} - \frac{k^2}{r^2}u = 0 \tag{22}$$

with the general solution:

$$u = C_1 \cdot r^k + C_2 \cdot r^{-k}$$

thus

$$\sigma_r = \frac{k^2\nu}{k^2\nu^2 - 1} E_r \left\{C_1(k\nu + 1) \cdot r^{k-1} - C_2(k\nu - 1)\, r^{-k-1}\right\}$$

$$\sigma_t = \frac{k^3\nu}{k^2\nu^2 - 1} E_r \left\{C_1(k\nu + 1) \cdot r^{k-1} + C_2(k\nu - 1)\, r^{-k-1}\right\} \tag{23}$$

With the boundary conditions:

$$(\sigma_r)_{r=a_1} = -p_i \qquad (\sigma_r)_{r=a_2} = -p_o$$

and

$$\alpha = \frac{a_2}{a_1}$$

we get the stresses

$$\sigma_r = \frac{a_1^2}{\alpha^{k-1} - \alpha^{-k-1}} \cdot \left\{ a_1^{-k-1} \cdot \left(p_i \alpha^{-k-1} - p_o\right) r^{k-1} - a_1^{k-1}\left(p_i \alpha^{k-1} - p_o\right) \cdot r^{-k-1} \right\} \tag{24}$$

$$\sigma_t = \frac{k \cdot a_1^2}{\alpha^{k-1} - \alpha^{-k-1}} \cdot \left\{ a_1^{-k-1} \cdot \left(p_i \alpha^{-k-1} - p_o\right) r^{k-1} + a_1^{k-1}\left(p_i \alpha^{k-1} - p_o\right) \cdot r^{-k-1} \right\}$$

The shear stress is maximum at the inner radius:

$$\tau_{max} = \frac{1}{2\left[\alpha^{k-1} - \alpha^{-k-1}\right]} \cdot \left\{ \left(p_i \alpha^{-k-1} - p_o\right)(k-1) + \left(p_i \alpha^{k-1} - p_o\right)(k+1) \right\} \tag{25}$$

The deformation of the insulation is calculated from:

$$u = C_1 \cdot r^k + C_2 \cdot r^{-k}$$

$$u = \frac{1}{k^2 \cdot \nu \cdot E_r (\alpha^{k-1} - \alpha^{-k-1})} \cdot \left\{ (k\nu - 1) \cdot a_1^{-k+1} \cdot \left(p_i \alpha^{-k-1} - p_o\right) \cdot r^k + (k\nu + 1) \cdot a_1^{k+1} \left(p_i \alpha^{k-1} - p_o\right) \cdot r^{-k} \right\} \tag{26}$$

In glass fiber-reinforced thermoset structures, the ratio $k^2 = E_t/E_r \neq 1$. The stresses σ_r, σ_t, and τ_{max} and the deformation u are calculated from variable values of α and k for the specific case of $a_1 = 5$ cm, $\nu = 0.35$ and $E_t = 7.5 \times 10^4$ kg cm^{-2}, and the boundary conditions (magnetic and thermal stresses) of $p_i = 100$ kg cm^{-2} and $p_o = 80$ kg cm^{-2} in Figs. 9a to 9d.

G. Electrical Stress Distribution in the Insulation

The conductor corners are rounded in order to ease manufacturing, handling, and insulation of turns in a coil. The radius of the rounded corner is generally determined empirically in relation to conductor dimensions.

The insulation thickness around each individual conductor and from conductor to ground is determined by considerations of safety in case of defects, voids, and pin holes in the insulation in order to provide enough distance between conductors and to prevent electrical breakdown. In the following, a mathematical treatment is given to calculate the electrical stress distribution in the insulation as a function of corner radius and insulation thickness.

The conductor geometries considered are illustrated in Figs. 10a and 10b.

The solution for the case of infinite conductor sides (Fig. 10c) is found from the modified Schwarz-Christoffel transformation, which assumes that the potential in the interspace follows the Laplacian $\nabla^2 \psi = 0$. The transformation equation from the t to the z plane is given by:

$$z = C_1 \int \frac{(1-\lambda)(t+a)^{\frac{1}{2}} + \lambda(t+1)^{\frac{1}{2}}}{t(t-b)^{\frac{1}{2}}}\, dt + C_2 \tag{27}$$

with $\lambda \geq 0$ as the parameter defining the contour. The solution of Eq. (27) is:

$$z = \frac{g}{\pi}(1-\lambda) \left\{ \ell n \frac{\left(\frac{t+a}{t-b}\right)^{\frac{1}{2}} + 1}{\left(\frac{t+a}{t-b}\right)^{\frac{1}{2}} - 1} - 2\left(\frac{a}{b}\right)^{\frac{1}{2}} \cdot \tan^{-1}\left(\frac{b}{a}\,\frac{t+a}{t-b}\right)^{\frac{1}{2}} - \ell n \frac{1 + \left(\frac{1-a}{1+b}\right)^{\frac{1}{2}}}{1 - \left(\frac{1-a}{1+b}\right)^{\frac{1}{2}}} - 2\left(\frac{a}{b}\right)^{\frac{1}{2}} \tan^{-1}\left(\frac{b}{a}\,\frac{1+a}{t-b}\right)^{\frac{1}{2}} \right\}$$

$$+ \frac{g}{\pi}\lambda \left\{ \ell n \frac{\left(\frac{t+1}{t-b}\right)^{\frac{1}{2}} + 1}{\left(\frac{t+1}{t-b}\right)^{\frac{1}{2}} - 1} - 2\left(\frac{1}{b}\right)^{\frac{1}{2}} \tan^{-1}\left(b\,\frac{t+1}{t-b}\right)^{\frac{1}{2}} \right\} \tag{28}$$

The equation of the quarter-circle defining the conductor corner is calculated from Eq. (28) to be:

$$x = \frac{g}{\pi}(1-\lambda) \left\{ \ell n \frac{1 + \left(\frac{t+a}{t-b}\right)^{\frac{1}{2}}}{1 - \left(\frac{t+a}{t-b}\right)^{\frac{1}{2}}} - 2\left(\frac{a}{b}\right)^{\frac{1}{2}} \cdot \tan^{-1}\left[\frac{b}{a}\,\frac{t+a}{t-b}\right]^{\frac{1}{2}} - \ell n \frac{1 + \left(\frac{1-a}{1+b}\right)^{\frac{1}{2}}}{1 - \left(\frac{1-a}{1+b}\right)^{\frac{1}{2}}} + 2\left(\frac{a}{b}\right)^{\frac{1}{2}} \tan^{-1}\left[\frac{b}{a}\,\frac{1-a}{1+b}\right]^{\frac{1}{2}} \right\} \tag{29}$$

$$y = g \left\{ 1 - \frac{2\lambda}{\pi} \tan^{-1} \left(\frac{1+t}{b-t} \right)^{\frac{1}{2}} + \frac{\lambda}{\pi (b)^{\frac{1}{2}}} \cdot \ell n \frac{1 + \left[\frac{b(1+t)}{b-t} \right]^{\frac{1}{2}}}{1 - \left[\frac{b(1+t)}{b-t} \right]^{\frac{1}{2}}} \right\}$$

For the corner shown in Fig. 10d,

$$\begin{aligned} x &= r \cdot \cos \phi \\ y - g &= r \cdot \cos \phi \end{aligned} \qquad (30)$$

With the boundary values:

$$\phi = \frac{3\pi}{2} \qquad x = 0 \qquad y = g \qquad t = -1$$

$$\phi = \pi \qquad x = -r \qquad y = g + r \qquad t = -a$$

we obtain a and b from the equation:

$$\frac{r\pi}{g} = \frac{1 - (b)^{\frac{1}{2}}}{1 + (b)^{\frac{1}{2}}} \cdot \left\{ \ell n \frac{1 + \left(\frac{1-a}{1+b} \right)^{\frac{1}{2}}}{1 - \left(\frac{1-a}{1+b} \right)^{\frac{1}{2}}} - 2 \left(\frac{a}{b} \right)^{\frac{1}{2}} \cdot \tan^{-1} \left[\frac{b}{a} \frac{1-a}{1+b} \right]^{\frac{1}{2}} \right\}$$

$$\frac{g+r}{g} = 1 - \frac{2}{\pi} \frac{(b)^{\frac{1}{2}} - (a)^{\frac{1}{2}}}{1 - (a)^{\frac{1}{2}}} \tan^{-1} \left(\frac{1-a}{b+a} \right)^{\frac{1}{2}} + \frac{1}{\pi (b)^{\frac{1}{2}}} \cdot \frac{b^{\frac{1}{2}} - a^{\frac{1}{2}}}{1 - a^{\frac{1}{2}}} \cdot \ell n \frac{1 + \left[\frac{b(1-a)}{b+a} \right]^{\frac{1}{2}}}{1 - \left[\frac{b(1-a)}{b+a} \right]^{\frac{1}{2}}} \qquad (31)$$

Figure 11 gives a and b values as a function of r/g and g/h. The electric stress across the insulation can be calculated from Eq. (3):

$$\frac{dW}{dz} = \phi + j\psi = \frac{\psi_o}{g} \cdot \frac{(t-b)^{\frac{1}{2}}}{\frac{1-(b)^{\frac{1}{2}}}{1-(a)^{\frac{1}{2}}} \cdot (t+a)^{\frac{1}{2}} + \frac{(b)^{\frac{1}{2}} - (a)^{\frac{1}{2}}}{1 - (a)^{\frac{1}{2}}} \cdot (t+1)^{\frac{1}{2}}} \qquad (32)$$

The stress on the conductor surface for various values of r/g is shown in Fig. 12.

Calculations of electric stresses for symmetric and perpendicular faces have been performed by Dreyfuss.[7] The breakdown voltage according to his calculation is proportional to the 2/3 power of the gap:

$$V_{BD} = C_1 \cdot g^{2/3} \qquad (33)$$

The breakdown voltage between two 90° perpendicular conductor surfaces with r/g = 0 is given as a modified Dreyfuss equation:

$$V_{BD} = C_2 \cdot g^{2/3} \cdot \left[1 + \left(\frac{g}{h} \right)^2 \right]^{1/6} \qquad (34)$$

If the corner radius $r \neq 0$, Eq. (33) needs further correction:

$$V_{BD} = C_3 \cdot g^{2/3} \left[1 + \left(\frac{g}{h} \right)^2 \right]^{1/6} \cdot \left[1 + \frac{g}{2r} \right]^{-1/3} \qquad (35)$$

The constants C_1 to C_3 can be calculated from boundary conditions unique for a special configuration. Experimental data show that the Dreyfuss equation and the modifications yield high stress values. However, as a first approximation, the equations are quite useful. For more accurate data, the calculated values of a and b (Fig. 11) for different values of g/h and r/g can be used in combination with Eqs. (29) and (32).

IV. Insulation Deficiencies and Their Effects

A. Voids and Insulation Failures

Voids in coil insulation may occur for different reasons. A common source is that the impregnant does not wet uniformly the glass fiber insulation and does not uniformly fill all voids between conductors or in ground insulation, due to lack of penetration of the thermoset into the glass fiber type, poor vacuum, trapped gas bubbles, high thermoset viscosity, or the tape itself, as shown in Fig. 13. With glass fiber tapes, the compatibility of the glass fabric with the thermoset is an important factor. The glass filaments have an oil dextrine surface finish and the wetting with epoxies is insufficient. The glass fiber must be heat-cleaned (to burn the oil starch finish) and treated chemically to restore part of the glass fiber strength reduced by the heat-cleaning process.[8] In case of vacuum impregnation, special care has to be taken when the vacuum is broken in order to reduce the jetting of air which can penetrate the thermoset bath and produce cavities or gas inclusions.

In the case of wet winding, or the use of semi-cured or B-stage insulation, the control of a uniform wetting throughout the coil is a difficult task. Common practices are preheating, application of vacuum (0.3 - 1 mm), subsequent pressure and a final pressing prior to curing by mechanical means, such as press plates, fixtures, hydraulic and pneumatic presses, or collapsible moulds. Even under the best circumstances it is difficult to produce a completely uniform impregnation.

A few voids of certain sizes may be harmless, but concentration and distribution of voids in specific areas close to the conductor edges may prove to be dangerous. In general, gas enclosures concentrate near the conductor corners due to shrinkage of the thermoset or in the presence of trapped gas. Between conductors it is frequently found that the impregnant does not penetrate thoroughly and wet the glass fiber cloth, which in case of water penetration into the insulation may prove disastrous. This case is often observed in bent portions of the coils, where the local surface pressure between conductors balances the pressure drop due to capillary forces, the pressure applied to the thermoset at the end of the impregnation process, and the final application of pressure by the mould prior to curing.

The coil impregnation occurs in three stages:

a. Penetration of the thermoset into the fibrous insulation. This penetration is due to a pressure drop, which may be expressed roughly as

$$\Delta p = 1/2\, \gamma\, v_o^2 \tag{36}$$

where γ is the density of the liquid thermoset and v_o the initial penetration velocity. If the width of the gap between fibers is Δ, the pressure drop per unit width due to capillary forces is expressed as

$$\Delta p = \frac{F_{cap}}{\Delta} = \frac{2\alpha \cdot \cos\phi}{\Delta} \quad . \tag{37}$$

Therefore,

$$v_o = \left(\frac{4\alpha \cos\phi}{\gamma\Delta}\right)^{\frac{1}{2}} \tag{38}$$

where α is the capillary constant and ϕ the brim or wetting angle.

b. Weight of the impregnant is added to capillary force. In this phase the influence of trapped air, which has to give way to the impregnant, is important. The trapped air may delay the wetting and subsequently the impregnation process. The importance of a good vacuum in this stage is quite obvious. Trapped air which can not escape can cause voids.

c. The last phase is determined by the weight, the external applied pressure (mostly atmospheric after breaking the vacuum), and the viscosity of the thermoset.

As may be seen from Fig. 14, the viscosity of the thermoset increases with time at the impregnation temperature. Thermosets with long pot life are preferred. The penetration process per unit width can be expressed as

$$F_{ext} + F_{cap} + \Delta(\gamma_{th} - \gamma_{air})\, x - \frac{12v\eta x}{\Delta} = 0 \tag{39}$$

and

$$\frac{dx}{dt} = v$$

with γ_{air} the density of air, γ_{th} the density of the thermoset, and η is the viscosity of the impregnant.

To calculate the differential Eq. (39) we use the boundary conditions that at time t 0 the penetration coordinate is x o, and at t t_k the viscosity of the thermoset is so high that the impregnation process is brought to a stop.

Assuming η and ϕ are constant over the impregnation period, we get from Eq. (39):

$$\Delta(\gamma_{th} - \gamma_{air}) \cdot x - F_{ex} + 2\alpha\cos\phi \cdot \ell n\left(1 + \frac{\Delta(\gamma_{th} - \gamma_{air}) \cdot x}{F_{ex} + 2\alpha\cos\phi}\right) = \frac{\Delta^3}{12\eta}(\gamma_{th} - \gamma_{air})^2 \cdot t \tag{40}$$

The penetration velocity may be given from Eq. (39):

$$v = \frac{\Delta}{12\eta}\left[\Delta(\gamma_{th} - \gamma_{air}) + \frac{1}{x}(F_{ext} + 2\alpha\cos\phi)\right] \tag{41}$$

The importance of F_{ext} and F_{cap} are obvious. At atmospheric pressure, the other terms of Eq. (41) are small compared to F_{ext}, which is shown in Fig. 15 as discontinuities of the velocity versus penetration depth curve for phases b and c. At impregnation phase b the external pressure is zero. The thermoset penetrates into the coil only by means of the capillary force and its own weight.

We calculate the penetration for different gap widths Δ, with the viscosity at 60^o C of an alumina-filled thermoset of $\eta = 10$ Poise or 1.07×10^{-3} gr · sec/cm^2. The density γ of the epoxy $\gamma \approx 2$ gr · cm^{-3}, density of air $\approx 1.19 \times 10^{-3}$ gr · cm^{-3} (at atmospheric pressure), the capillarity constant $\alpha \approx 60 \times 10^{-3}$ gr/cm, and the brim angle is approximately 20^o, in Fig. 16.

For large coils with a long impregnation period, the brim angle ϕ and the viscosity η are changing with time. Equation (39) may be expanded accordingly and integrated for each special case.

Another source of void production is the internal stress due to exotherm reaction of the resin. This effect is enhanced when pure epoxy is accumulated in spots without the reinforcement of glass filaments and there are different expansion coefficients of the conductor material and the impregnant. During curing the polymerization passes through a critical stage, and a sudden temperature rise due to exotherm reactions can lead to local tension and cracks. The curing of large quantities of epoxy must be performed by a precuring at temperatures equal to impregnation temperature or lower until the thermoset is gelled, followed by a post curing.

In a uniform casting, external stresses due to different coefficients of expansions between conductor and the thermoset, temperature gradient between adjacent conductors, temperature fluctuations (cycling), electromagnetic and mechanical forces, and surface corrosion due to the presence of moisture and nuclear radiation may lead to early fatigue and damage of the insulation. In the absence of moisture, even if the insulation has been mechanically damaged, the insulation resistance may be high and the coil can operate satisfactorily. However, because some water is always

present, the breakdown voltage is reduced to a fraction of its initial value.

Magnet coils must be able to operate in a radiation environment. The radiation leads to ionization and oxidative degradation, polymerization and depolimerization, breaking of covalent forces, double bond formation cross linking, and displacement of atoms.

Several of these reactions may occur simultaneously, but the initial effect is a fast heterogeneous curing process, which improves tensile, flexural and shear strengths, but the effect of fast neutrons results in a highly cross-linked binder which is fragile and crash-sensitive. The binder cannot withstand mechanical forces, becomes brittle, and disintegrates into a black powdery substance. The binder is now more susceptible to oxidation and moisture absorption.

In numerous cases, coil insulations exposed even to moderate integrated radiation levels ($\leq 10^9$ rads) have failed, and flashover and breakdown have occured at levels of only a few volts.

The irradiation damage has been investigated previously,[1] but corona and dielectric breakdown are treated below more in detail.

B. Corona

The gradual increase of applied voltage across an insulation having voids and fissures causes the insulation to exhibit discharges called corona threshold at a certain voltage. If the cavity in the insulation contains oxygen, due to electric discharges, ozone is produced which oxidizes the material and extends the region of destruction until breakdown between conductors may occur. The duration of one discharge is of the order of 10^{-8} sec. If the discharge energy has been used up, the ionization and the discharge stop. If the applied voltage over the insulation is kept constant, the discharge repeats itself with a frequency of 10 to 100 megacycles. A decrease of applied voltage stops corona, but if the voltage is increased after a short period of time, say a few seconds, the corona threshold is lower than in the first discharge. This may be due to the primary electron avalanche in the cavity, which has not come to a complete stop in the thermoset.

The discharge phenomena can be explained by means of an analogy model shown in Fig. 17. If C_1 is the capacity across the cavity in a force tube, C_2 the capacity of the sound insulation, C_3 the capacity of the rest of the sound dielectric, and V_m the applied voltage, the ionization phenomena can be explained as follows:

When the voltage reaches a certain value V_{11} the discharge is initiated. After a certain time the voltage at C_1 is V_{10} and the discharge stops. If V_1 is the voltage across C_3, we get:

$$V_{11} = \frac{C_2}{C_1 + C_2} \cdot V_1 \qquad V_{21} = \frac{C_1}{C_1 + C_2} \cdot V_1 \tag{42}$$

and the voltage across C_3 after the discharge is

$$V_0 = \frac{C_1C_2 + C_2C_3 + C_1C_3}{(C_1 + C_2)(C_2 + C_3)} \cdot V_1 + \frac{C_2}{C_2 + C_3} \cdot V_{10} \tag{43}$$

The discharge creates a voltage drop over the cavity, which is given by

$$\Delta V = V_0 - V_1 = -\frac{C_2}{C_2 + C_3} \cdot (V_{11} - V_{10}) \tag{44}$$

For $C_2 \ll C_3$ the voltage drop is small.

The electric charge which is transferred from C_3 to C_1 during the discharge is given by

$$\Delta Q = C_3 \Delta V = -\frac{C_2 C_3}{C_2 + C_3} \cdot (V_{11} - V_{10}) \tag{45}$$

V_1 and V_0 are dependent on the voltage polarity at the cavity.

Each discharge represents a loss of energy and is constant as long as the applied external voltage does not change. The charge in electrostatic energy in the capacitive circuit is compensated during the discharge by Joule's heating in the cavity surface element and along the path of the discharge, and can be expressed as:

$$W_R = \frac{C_1C_2 + C_2C_3 + C_1C_3}{2(C_2 + C_3)} \cdot (V_{11}^2 - V_{10}^2) \tag{46}$$

The frequency of the dielectric discharges is so high that no voltage fluctuation across the power supply terminals can be observed. The energy supplied by the voltage source is $V\Delta Q$.

If many cavities are distributed over a tube of force, the energy is expressed as:

$$W = \sum_{\nu} \sum_{\mu} V_{\nu\mu} \cdot \Delta Q_{\nu\mu} \tag{47}$$

where, ν notates all discharges in a single void and μ is the summation over all cavities.

Corona discharges are generally destructive in magnet insulation, primarily because of the generation of ozone and various nitrogen compounds that attack the metal and the thermoset. The chemical destruction is the reaction of three available materials, oxygen, nitrogen, and water.

Condensation water can penetrate the insulation, where the presence of water leads to formation of nitric and nitrous acids. The latter attacks copper, and ozone the insulation. The Joule's local heating on the cavity surface due to corona accelerates the aging of the organic binder and lowers the dielectric strength. Mica is corona-insensitive and therefore very attractive for use in coil insulation, even if the initial strength of the mica-loaded tape is somewhat lower than the glass fiber epoxy matrix.

As pointed out, the corona frequency is of the order of megacycles. However, the frequencies are randomly distributed and their filtering is not possible. We know that it is practically impossible to eliminate all voids in a coil, but we can design the magnet so that the applied voltage to the coil and subsequently the interturn voltage is lower than the corona threshold. However, in cases of surge voltages, corona may occur, and due to the fact that after the initial corona discharge the corona threshold value is reduced, the corona discharges may continue even at operational voltage.

Corona measurements with glass fiber epoxy matrices (i.e., medium-weave, glass fiber, Volan A-treated, Union Carbide ERL 2256 epoxy and MPDA hardener) of 0.1 cm thickness between two conductors gave a corona threshold value of 14 kV/cm $\pm$ 8% in dry conditions and 10.8 kV/cm $\pm$ 13% after 24 hours immersion in tap water. Where voids (0.01 cm gap width) were present, the threshold value measured was 2.52 kV/cm $\pm$ 18% and after a 24-hour immersion, 1.17 kV/cm $\pm$ 22%.

The evaluation of the corona threshold is characterized by a sharp knee in the charge versus applied voltage curve. Oscillograms of corona measurements are illustrated in Fig. 18.

The corona threshold is observed on the oscilloscope as high frequency pulses or as "grass." If the applied voltage is gradually increased, the pulses have higher energy levels and partial discharges can be observed. If the applied voltage is further increased, the discharges become dense and insulation breakdown may occur.

C. Delamination

Delamination of insulation may occur for several reasons; high shear stress may be produced between adjacent conductors, which may exceed the bond strength of the thermoset. Generally, the thermosetting is sheared off from the conductor surface, causing cavities and initiating corona around the conductor edges. If moisture is present in the coil environment, water can penetrate the insulation and fill the area around the conductor. If the conductor is heated by Joule's losses, the water may evaporate and cause further opening of the fissures and cracks, which gradually may lead to insulation breakdown.

Delamination may occur due to the reduction of the elasticity modulus at high temperatures (Fig. 5) and reduction of the bond strength. Ionization caused by irradiation and corrosion in the presence of moisture may also cause delamination. Delamination occurs due to large deviations in the values of elastic moduli E_r and E_t.

V. Insulation Testing

Generally, powerful dc magnets are low-voltage, high-current devices. Alternating-gradient ac magnets use high voltage, and their insulation problem therefore is more complicated. A test program covering all possible insulation failures for dc or ac magnets, respectively, will be beyond the scope of this paper. However, the most important nondestructive tests for both magnet categories are discussed below.

A. High Frequency Test

The voltage applied to the coil terminals, or induced, has a frequency of about 400 to 800 cps. The reason for the high frequency is to stress the turn-to-turn insulation electrically to about 50-200 volts between turns. This test has the following features:

a. In case of interturn shorts or insulation failures, the specific coil section is heated.
b. The coil manufacturer may control the soundness of insulation during the winding and insulation process, prior to and after the impregnation and curing.

B. High Voltage Ground Insulation Test

A high dc or ac voltage is applied to the terminals while the insulated portions of the coil are covered by shot , metallic foil, or tap water. If the coil has been immersed in water for several hours, the latter test is very effective in detecting any surface corrosion, ground insulation voids, or other deficiencies.

C. Circuit-to-Circuit High Voltage Test

Coils of large electromagnets are multifilar-wound. After the thermoset is cured, high voltage is applied to one circuit with the second circuit grounded. This method is extremely useful in finding any insulation damage in the transition areas between pancakes, where the insulation is easily ruptured during manufacturing.

Larger coils are mostly multifilar-wound in order to reduce the water pressure drop across each hydraulic circuit. The circuits can be connected electrically after the high voltage test.

D. Insulation Thickness Test

A number of devices have been developed recently to check the ground insulation thickness without cutting through the insulation. Common devices are:

1. Eddy current device.
2. Radiation back scather device.
3. Ultrasonic device.

E. X-Ray and Betatron Tests

Although this is quite a complicated and, in large coils, an impractical process, x-ray pictures can be taken of coil portions in order to detect voids.

F. Impulse Test

The reason behind introducing impulse testing in dc magnets is only to have a highly sensitive method to measure failure in coil insulation, which can not be detected by means of the classical high-frequency and loss factor measuring techniques. The impulse test can be applied to dry or wet coils, as desired.

The voltage distribution in magnet double pancakes can be derived from measurements and calculations with transformer coils.

The winding diagram of Wagner[10] is used as a basis when studying the behavior of the impulse wave in a magnet coil. Although we know that this diagram neglects the influence of the mutual inductance between turns and between coils and the core, it gives a qualitatively good picture which corresponds with measured results.

The turns of a magnet coil are capacitively coupled with one another. Figure 19 illustrates the equivalent

diagram of the winding. When an impulse wave infringes upon such a winding, it is possible to differentiate between three different phases in the behavior of the impulse wave:

1. The initial distribution caused by the steep front of the impulse wave.
2. The final distribution, which is produced by the weak voltage changes at the end of the impulse wave tail.
3. Transient oscillations, as phenomena from the initial distribution to the final distribution of the impulse wave.

For a coil with one terminal grounded and the impulse voltage applied to the other, the voltage distribution follows the equation:

$$\frac{\partial^2 V}{\partial x^2} - \frac{L}{C_g}\frac{\partial^2 V}{\partial t^2} - LC_w \cdot \frac{\partial^4 V}{\partial x^2 \partial t^2} = 0 \qquad (48)$$

The equation describes the transient phenomena of the impulse wave in the interior of the coil. Its solution is known to be:

$$V = V_m \cdot e^{j\omega t} \cdot e^{jkx} \qquad (49)$$

The differential equation of the initial distribution,

$$V_i = V(x, o) \qquad (50)$$

is obtained when the inductance L per unit length in the equivalent circuit diagram, Fig. 19, is not considered.

When $L \rightarrow \infty$, Eq. (48) becomes:

$$\frac{\partial^2 V}{\partial x^2} = \frac{C_g}{C_w} \cdot V_i \qquad (51)$$

At the high voltage end of the winding,

$$x = \ell \text{ and } V = V_{imp} .$$

When the coil is grounded,

$$x = 0 \qquad V = 0$$

We obtain from Eq. (51) the equation for the voltage distribution along the coil:

$$V_i = V_{imp} \cdot \frac{\sinh\left(\frac{C_g}{C_w}\right)^{\frac{1}{2}} \frac{x}{\ell}}{\sinh\left(\frac{C_g}{C_w}\right)^{\frac{1}{2}}} \qquad (52)$$

The voltage gradient amounts to:

$$\frac{\partial V_i}{\partial x} = \frac{\left(\frac{1}{\ell} \cdot C_g/C_w\right) \cdot V_{imp} \cosh\left[\left(\frac{C_g}{C_w}\right)^{\frac{1}{2}} \frac{x}{\ell}\right]}{\sinh\left(\frac{C_g}{C_w}\right)^{\frac{1}{2}}} \qquad (53)$$

The maximum voltage gradient occurs at the terminals, i.e., at $x = \ell$:

$$\left(\frac{\partial V_i}{\partial x}\right)_{max} = \frac{1}{\ell} \cdot \left(\frac{C_g}{C_w}\right)^{\frac{1}{2}} = \frac{\alpha_i}{\ell} \qquad (54)$$

where

$$\alpha_i = \left(\frac{C_g}{C_w}\right)^{\frac{1}{2}} \qquad (55)$$

Curves of initial voltage distribution are given in Fig. 20.

The final distribution of the impulse wave appears when the voltage changes at the wave tail are small. In this case no current flows through the capacitance elements and the inductive elements control the current. The conductor resistance is neglected. The differential equation for the final distribution is obtained from Eq. (48) :

$$\frac{\partial^2 V_f}{\partial x^2} = 0 \qquad (56)$$

$$V_f = Ax + B$$

with $x = \ell$, $V = V_{imp}$, $x = 0$, $V = 0$,

$$V_f = V_{imp} \cdot \frac{x}{\ell} \qquad (57)$$

The current flowing through the coil is obtained from Fig. 19.

$$\frac{\partial V}{\partial x} = - L \frac{di}{dt} \qquad (58)$$

$$i = \frac{V_{imp}}{\ell \cdot L} t \qquad (59)$$

The transition from initial to final distribution takes place in the form of transient oscillations. The energy of these oscillations is the difference between the electrostatic energy of the initial and final distribution. The voltage to ground reaches its crest during this transient period.

When we proceed from the rectangular impulse wave, we obtain from Eq. (48) the expression for the sum of all free partial oscillations:

$$V_{Tr} = V_{imp} \sum_n \left(A_r e^{j\beta_n x} + B_n e^{-j\beta_n x}\right) e^{j\omega_n t} \qquad (60)$$

A_n and B_n are integration constants. With the conditions that at $x = \ell$ the voltages V_i as well as V_f are equal to the applied impulse voltage V_{imp}, the expression valid for the entrance to the winding at any time is given by $V(o,t) = V_{imp}$ and for the grounded end, $V(\ell, t) = 0$

$$V_{Tr}(x,t) = V_{imp} \cdot \sum (A_n \cdot \cos\beta_n x + B_n \sin\beta_n x) \cdot \cos(\omega_n t) \tag{61}$$

With the boundary values:

$$A_n = 0 \qquad \beta_n = \frac{n\pi}{\ell}$$

$$B_n = -\frac{2}{n\pi} \cdot \frac{\alpha^2}{(n\pi)^2 + \alpha^2}$$

$$n = 1, 2 \ldots$$

we get the equation of the free oscillations:

$$V_{Tr}(x,t) = V_{imp} \cdot \frac{x}{\ell} + 2V_{imp} \sum_{n=1}^{n} \frac{2}{(n\pi)^2 + \alpha^2} \cdot \sin \frac{(n\pi x/\ell)}{n\pi} \cdot \cos \omega_n t \tag{62}$$

and the equation of the envelope:

$$V_{Tr}(x) = V_{im} \cdot \frac{x}{\ell} + V_{im} \sum_{n} \frac{2\alpha^2}{(n\pi)^2 + \alpha^2} \cdot \frac{\sin n\pi x/\ell}{n} \tag{63}$$

Figure 21 illustrates the calculated transient oscillations and the envelope. The calculated curves can be compared with experimental tests.

In all the above equations α or the ratio of the series to the ground capacitance is of primary importance.

The series capacitance of a coil is defined as the capacitance which would store the same electrostatic energy as the coil itself. Assuming that the voltage distribution over a double pancake is linear, the series capacitance of a disk coil winding with N double pancakes connected in series is given by

$$C_w = 8.859 \left\{ \frac{\epsilon_r \cdot \ell_m \cdot h}{d \cdot (n-1)N} + \frac{4}{3} \cdot \frac{\epsilon_r \ell_m \cdot (b)}{\Delta \cdot N} \right\} \text{ (pF)} \tag{64}$$

The ground capacitance depends on the coil geometry and the relative dielectric constant surrounding the coil:

$$C_g = \frac{8.859 \cdot N \cdot \sum_{\nu=1}^{m} \ell_\nu \cdot h_\nu}{\sum_{n=1}^{n} \frac{d_n}{\epsilon_n}} + \frac{2\pi \cdot 8.859 \cdot N \cdot h_\nu}{\ell n \frac{R}{r}} \text{ (pF)} \tag{65}$$

where all linear coil dimensions are in meters. By means of the above treatment, we can calculate the voltage and current distribution for an impulse voltage of rectangular shape or a steep front and long tail. The advantage of impulse testing magnet coils is in detecting even small insulation failures. Partial shorts covering a few percent of the coil length can be detected using sensitive measuring and detecting methods. The experience gained in testing transformer coils can be adapted in magnet coils in full. The impulse methods described below give qualitative results and are not necessarily due to subjective experience and judgment. The impulse testing can be performed on the whole coil installed in the magnet; however, we suggest testing each coil section separately. The coil can be placed between parallel plates and the impulse circuit shown in Fig. 22 may be chosen. When plates and one terminal are grounded over high precision shunts, current and voltage oscillograms will indicate sound coils, corona, and insulation defects. Current oscillograms from a magnet coil taken with the impulse tester are shown in Fig. 23.

The impulse testing will be performed in the following way:

1. Impulse voltage of reduced amplitude is applied to each coil terminal, grounding the other.
2. Full impulse voltage is applied to each coil terminal, grounding the other terminal.
3. The voltage and current oscillograms are compared, as well as the oscillogram of current flowing through the plates, which will reveal any insulation failure.

At present the impulse testing of magnet coils is in a preliminary stage. Acquisition of an appropriate impulse tester, and standarization of the shape duration and maximum amplitude are necessary. But from past and present experience with the highly-alumina-filled thermosets used in SLAC coils, we feel that the impulse testing is essential. SLAC specifies a maximum impulse voltage of 20 times the operational voltage with an impulse wave of 1 μs risetime and 50 μs half decay time. However, these values may seem arbitrary and need further detailed investigation.

G. Corona Test

Besides the measurement of the insulation loss factor with a Schering bridge to determine the tan δ values of dry and wet insulation, and the impulse testing, the measurement of the corona threshold has been introduced in judging the soundness of coil insulations.

The corona avalanche intensity can be defined as the apparent intensity of the reoccuring pulse in the oscilloscope. The pulse height is converted from

centimeters into apparent microcoulombs by application of a calibration constant obtained by charging the coil to a known direct voltage and connecting the charged coil to a suitable corona tester. The height of the resulting voltage transient is observed on the oscilloscope and is converted to a sensitivity figure K for the circuit through use of:

$$Q = C \cdot V$$

$$= C \frac{V}{h_1} \cdot h_2 \qquad (66)$$

$$= K \cdot h_2$$

with h_1 the height of the calibration pulse, h_2 the height of the pulse on the oscillogram, C the capacitance of the coil, and V the applied voltage.

From different test methods such as the NEMA noise tester,[11] the Hissing method,[12] and the Quinn resonant circuit method,[13] we mention two methods which have been used at SLAC for coil testing:

1. The tester shown in Fig. 24a has been used. The coil, or test sample A, is connected over a grounded coaxial cable to a variable oscillation damper C and amplifier D, a calibrator E and an oscilloscope F. The detailed circuit diagram is shown in Fig. 24b.

The high-frequency corona discharge oscillations pass through a filter and are monitored in the oscilloscope.

Figure 25 illustrates the corona threshold of some sound and faulty coil insulations as a function of the applied ac voltage.

2. The impulse tester shown in Fig. 26 uses a simple LC circuit as an indicator. Only the high-frequency discharges are monitored by the oscilloscope. The dc or low-frequency oscillations are blocked by the capacitance C.

Both impulse testers are operated on the grounded side of the coil. It may be pointed out that, due to the required high sensitivity of the test apparatus, the corona tester set up must be screened from the environment. The high voltage leads as well as the connectors must be shielded by means of copper tubings and metallic balls. Corona-free, double-shielded, high voltage cables are recommended as connections.

VI. Conclusions

Coils and their insulations can be regarded as the most delicate parts of a magnet. Their soundness guarantees the lifetime of a magnet and insures smooth and trouble-free operation in combination with accelerators. With the development of high-energy accelerators, the stresses on conductors and coil insulations are increasing. To comply with the requirements in accelerators regarding lifetime and reliability, the insulation methods and techniques, as well as insulation materials, have been improved markedly in recent years. The demand for better coils makes it necessary that reliable insulations must be used in coils and nondestructive test methods improved. At present, each laboratory judges the test procedures and coil performance from its own experience. A suggestion to standardize the test methods in order to obtain better judgment and collect test data which may be used by a larger number of magnet engineers and manufacturers concludes this report.

References

1. H. Brechna, "Effect of Nuclear Radiation on Organic Materials, Specifically Magnet Insulations in High-Energy Accelerators," SLAC Report No. 40, Stanford Linear Accelerator Center, Stanford, California, (March 1965).

2. S. Oleesky and G. Mohr, Handbook of Reinforced Plastics (Reinhold Publishing Co., New York, 1964).

3. S. Timoshenko, Strength of Materials, Part II (D. Von Norstrand Co., Inc., New York, 1950).

4. H. Brechna and W. Haldemann, "Physical Properties of Filament-Wound Glass Epoxy Structures as Applied to Possible Use in Liquid Hydrogen Bubble Chambers," presented at the 1965 Cryogenic Engineering Conference, Rice University, Houston Texas, August 23-25, 1965.

5. H. P. Hernandez, "Hollow conductor Magnet Pancake Cooling with Axial Conduction," Berkeley Engineering Note UCID 1779 Rev. 1, University of California, Berkeley, California (Oct. 25, 1962).

6. S. Timoshenko, Strength of Materials, Part I (D. Von Norstrand Co., Inc., New York, 1950).

7. L. Dreyfus, "Ueber die Anwendung der Theory der Konformen Abbildung zur Berechnung der Durch schlag-und Ueberschlagspannung zwischen kantigen Konstruktions-teilen unter Oel," Arch. Elektrotechnik Bd XIII, 123 ff. (1924).

8. W. J. Eakins, The Interface: The Critical Region of a Composite Material (to be published).

9. K. W. Wagner, "Das Eindringen einer elektromagnetischen Welle in eine spule mit Windungskapazitaet," E and M (1915) p. 89 ff.

10. H. Brechna, "Impulse Voltage Proof Transformer Windings," Recent Developments in Transformer Design, Oerlikon Engineering Co. Report p. 23 ff.

11. NEMA, "Methods of Measuring Radio Noise," NEMA Publication No. 107 (1940).

12. S. Whitehead, Dielectric Breakdown of Solids, (Oxford University, Pren, London, 1951), Cap. IV.

13. W. T. Starr, "Corona Properties of Insulating Materials," Electrical Manufacturing, Vol. 57, (1956).

14. J. H. Hagenguth, "Progress in Impulse Testing of Transformers," Trans. Eleck, Eng. Dec. Supplem. 63, 999, 1444 (1944).

FIGURE CAPTIONS

Insulation Structure and Coil Reliability

1a. Cross section through a double pancake. The hollow conductors wrapped in medium-weave, Volan A-treated glass cloth are impregnated in alumina-filled epoxy. Ground insulation is an open weave.

1b. Cross sectional view through the 0.1^{o} pulsed magnet coil. The coil is impregnated under vacuum in two stages. The cable is impregnated under vacuum with an epoxy composite of low viscosity. The coil is cast in highly filled thermoset in an open mold. Both thermosets are cured in the same process.

2. Two-dimensional double pancake for the 3^{o} SLAC bending magnet, manufactured by General Electric.

3. Three-dimensional coil for the Cornell University Panofsky quadrupole. (By courtesy of Pacific Electric Motors).

4. Two-dimensional coil geometry:
   a. Cross section through a corner
      1. Insulation
      2. Conductor
      3. Coolant passage
   b. Coil neutral axis
   c. Stress distribution in the insulation.

5. Variation of the modulus of elasticity for tension of a glass fiber, asbestos, epoxy matrix as a function of temperature.

6. Insulation tester. A coil section is held in the test fixture and the insulation sheared by the ram head.

7. Pancake to test mechanical and electrical properties of the insulation.

8. Stress distribution over a double pancake due to thermal gradient between adjacent conductors.

9a. Radial stress distribution in the insulation for various insulation thicknesses.

9b. Tangential stress distribution in coil insulation.

9c. Shear stress as a function of $k = (E_t / E_r)^{\frac{1}{2}}$.

9d. Radial insulation deformation.

10. Model for calculation of dielectric stress in insulation.

11. Parameters a and b as function of r/g and g/w.

12. Dielectric stresses over the conductor corner.

13. Cross section through a pancake. Voids due to impregnation deficiencies are clearly visible.

14. Viscosity curves as a function of temperature and time.
    1. DER 332 LC; Hardener: MDA, 7 p.p.w; MPDA, 11 p.p.w; Alumina filler, 325, 100 p.p.w; Cab-o-sil, 1 p.p.w; Z-6040, 1 p.p.w. Both temperature maintained throughout test: 70°C.
    2. As in case (1) with bath temp. 60°C ± 1°C.
    3. As in case (1) with bath temp. 50°C ± 1°C.
    4. As in case (1) with bath temp. 50°C ± 1°C.
    5. As in case (1) with bath temp. 38°C ± 3°C.
    6. Araldite 6005 (F), 100 p.p.w; Hardener 906 (NMA), 80 p.p.w; Accelerator 062 (BDMA), 2 p.p.w. Ciba Corp.

15. Speed of thermoset as function of penetration depth. The gap width is used as parameter. The epoxy formulation used was: DER 332 LC, 100 p.p.w.; Hardener, MDA, 7 p.p.w.; Accelerator, MPDA, 11 p.p.w.; Filler: Alumina, 325 mesh, 110 p.p.w.

16. Thermoset penetration as a function of impregnation time for constant and variable viscosity.

17. Model to determine corona threshold.

18. a. Corona threshold measured in a double pancake.
    b. Corona discharges in a double pancake with several randomly distributed small voids.

19. Equivalent diagram of a double pancake after Wagner
    ℓ: Length of a double pancake (or a coil)
    L: Inductance per unit length
    C_w: Series capacitance of a double pancake
    C_g: Ground or shunt capacitance of a double pancake.

20. Initial impulse voltage (V_{imp}) distribution in a double pancake with one grounded terminal.

21. Transient oscillations and the voltage envelope.

22. Impulse tester according to Hagenguth (Ref. 14).
    C_1: Charging capacitance
    SG: Spark gap or ignitron.
    R_1: Damping resistance.
    C_2: Load Capacitance.
    R_2: Discharge resistance.
    C_oC: Coaxial cable.
    R_3: High precision shunt.

23. Current oscillograms taken with the Hagenguth[14] impulse tester over a coil.
    a. Current through the coil with reduced voltage.
    b. Current with full impulse voltage.
        1. Corona discharges.
        2. Insulation breakdown.

24. a. General diagram of a corona tester.
    b. Corona tester according to Messwandlerbau Bamberg (Germany).

25. Corona discharge curves vs applied ac voltage.
    1. Sound double pancake.
    2. Useful insulations having few voids.
    3. Insulation with several randomly distributed voids (may be reliable if used in dry environment).
    4. Unreliable coil insulation with many voids.

26. Corona measurement device according to Brechna.

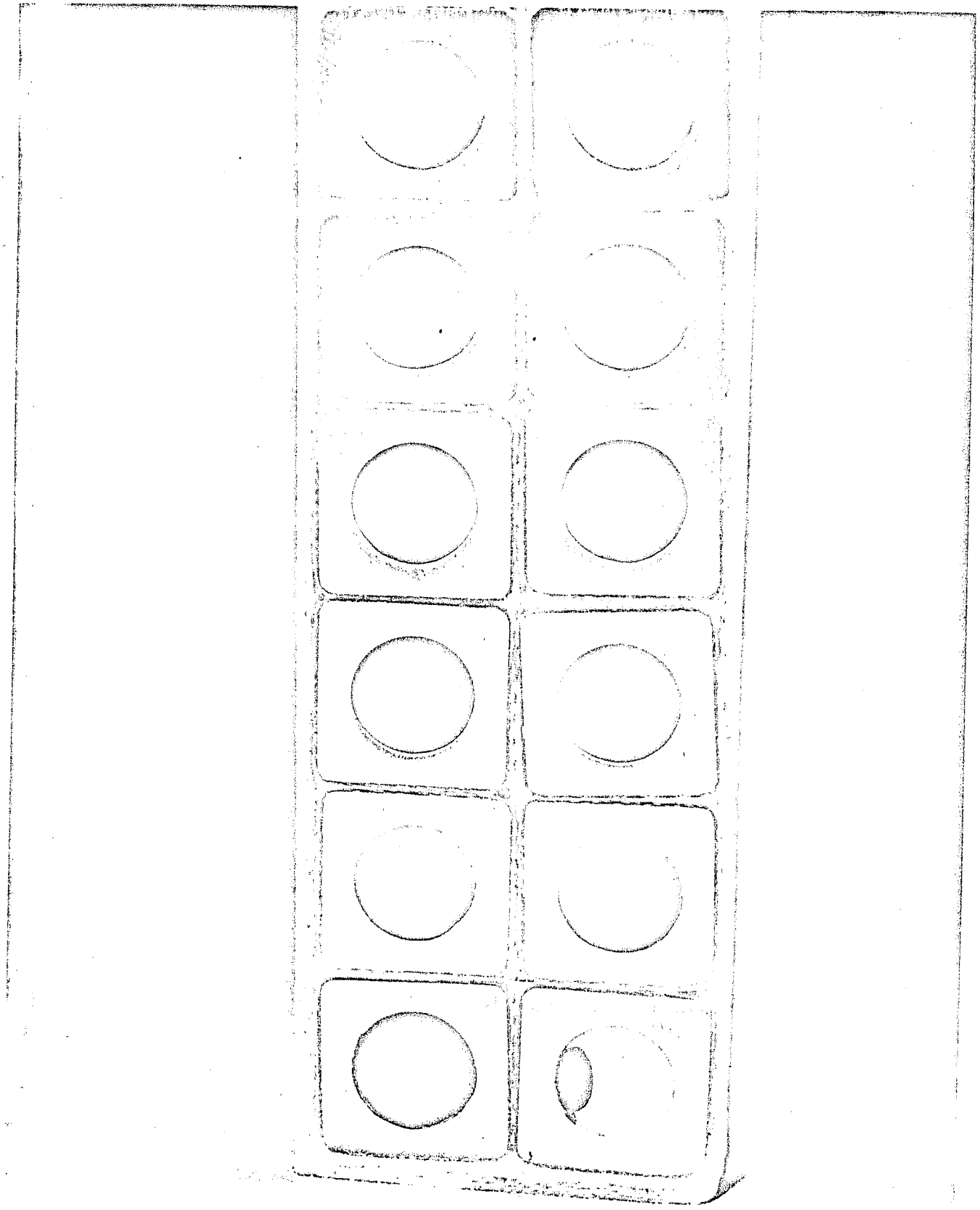

369-10-A

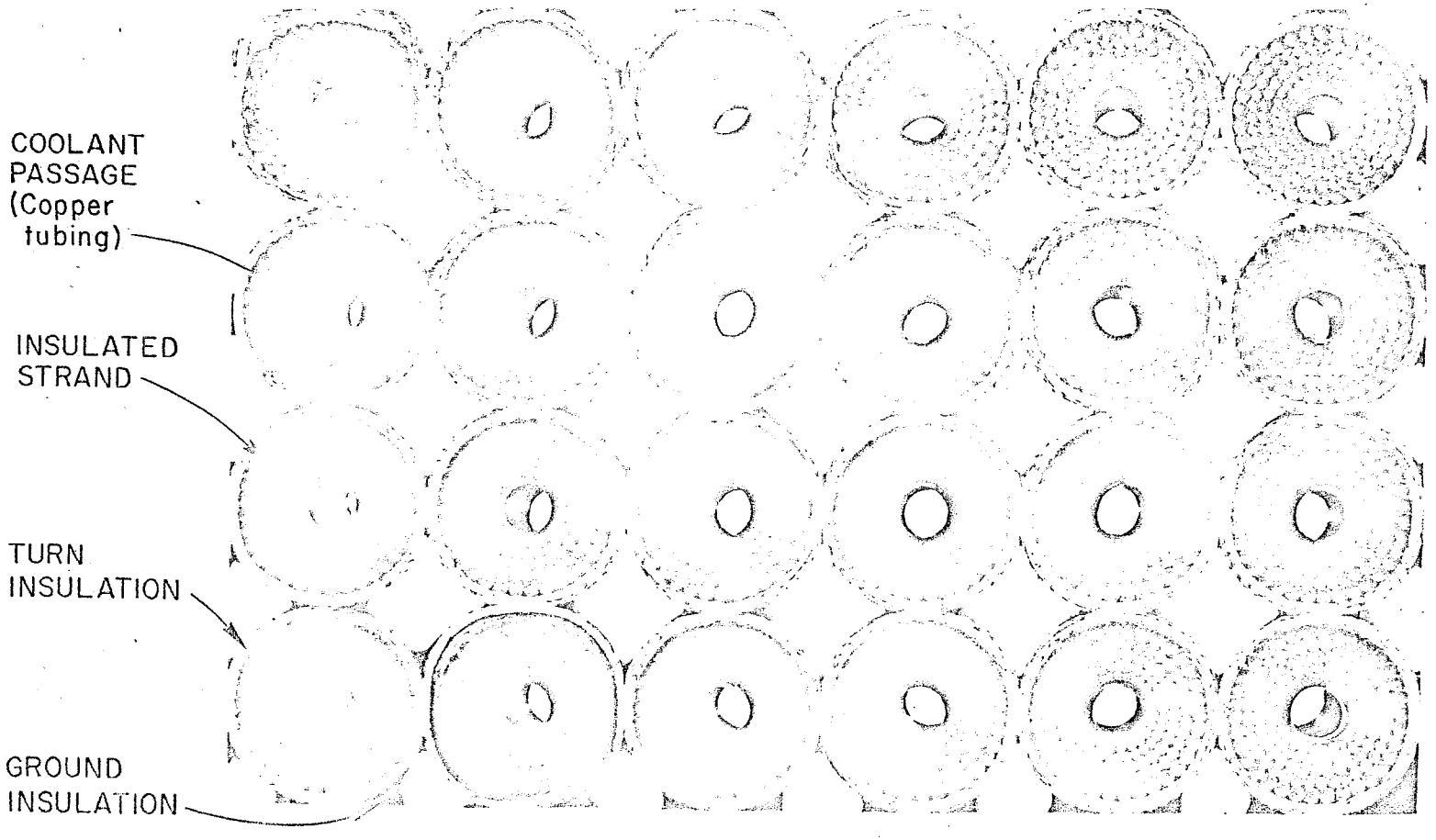
COOLANT
PASSAGE
(Copper
tubing)
INSULATED
STRAND
TURN
INSULATION
GROUND
INSULATION

369-14-A

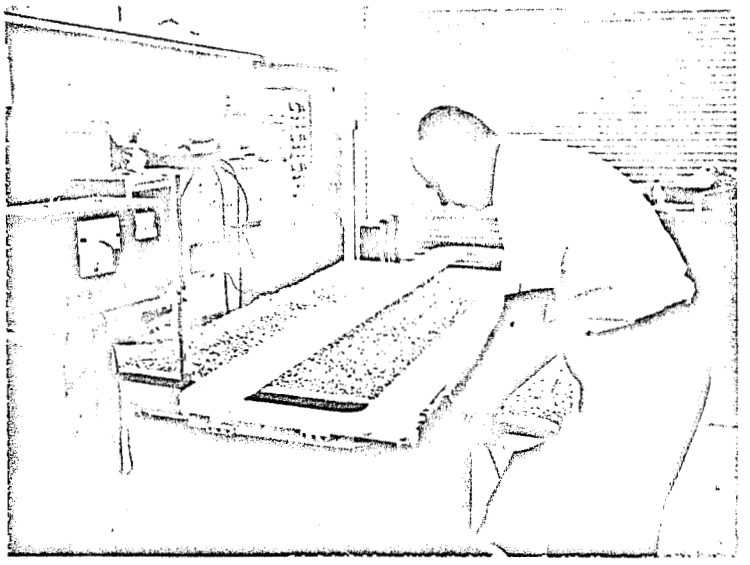

369-16-A

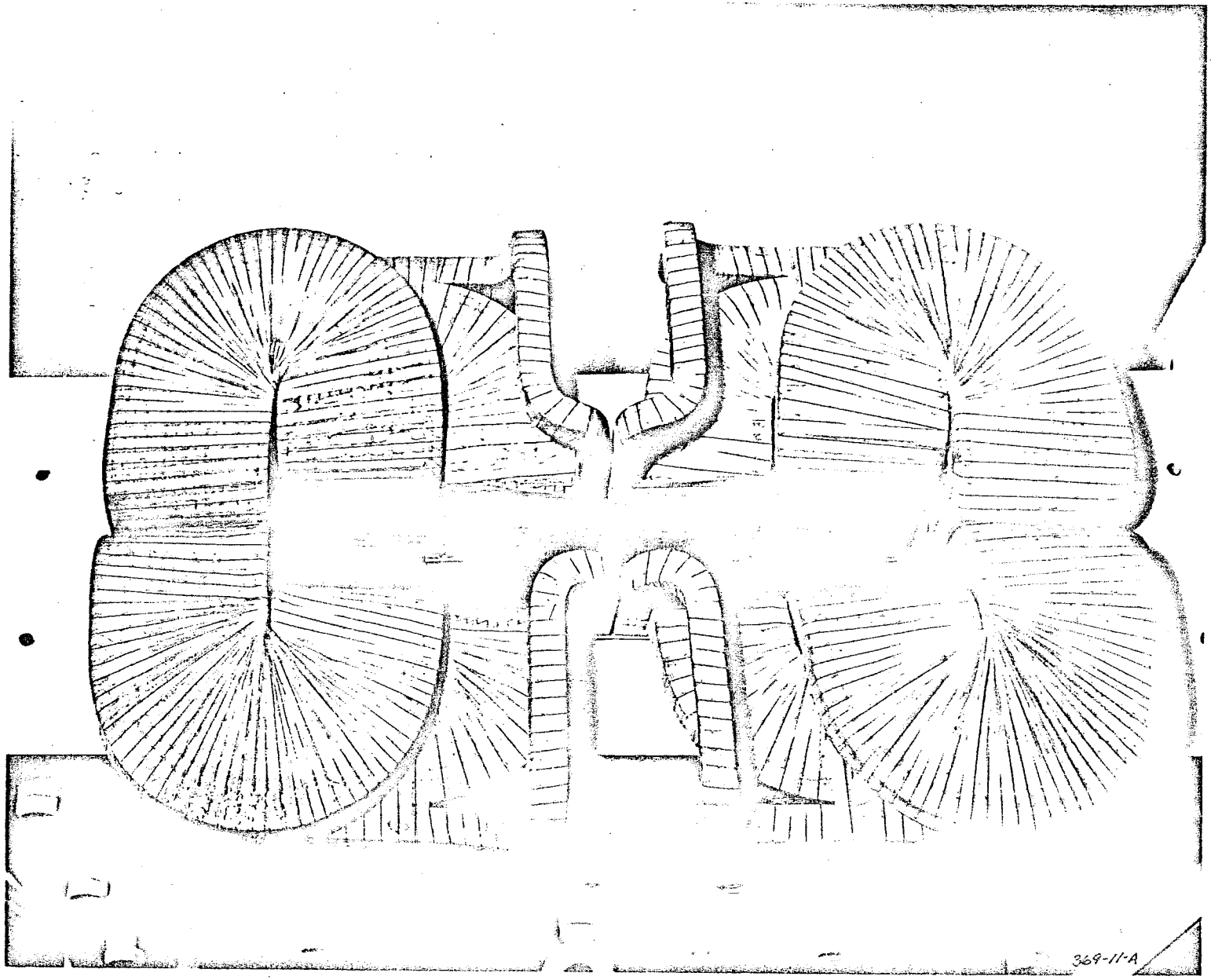
369-11-A

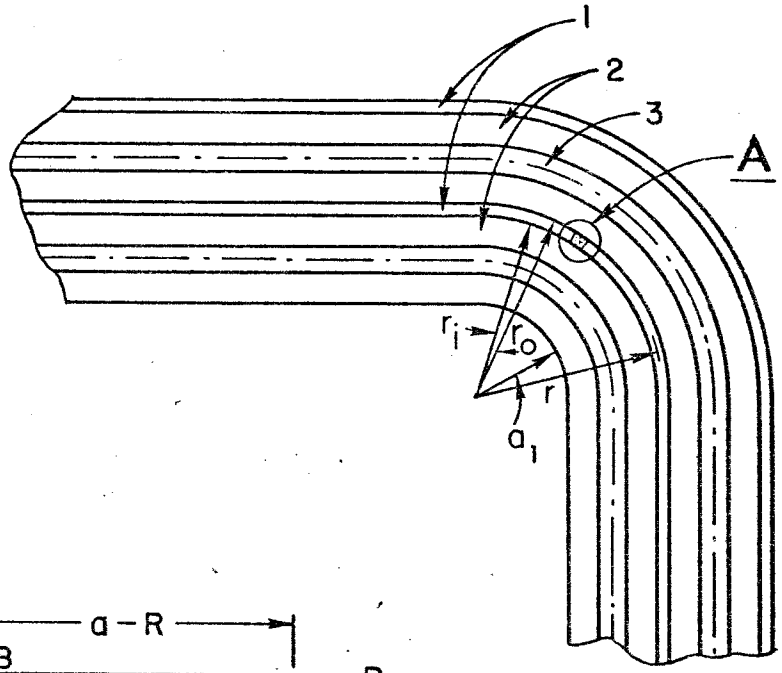

a)

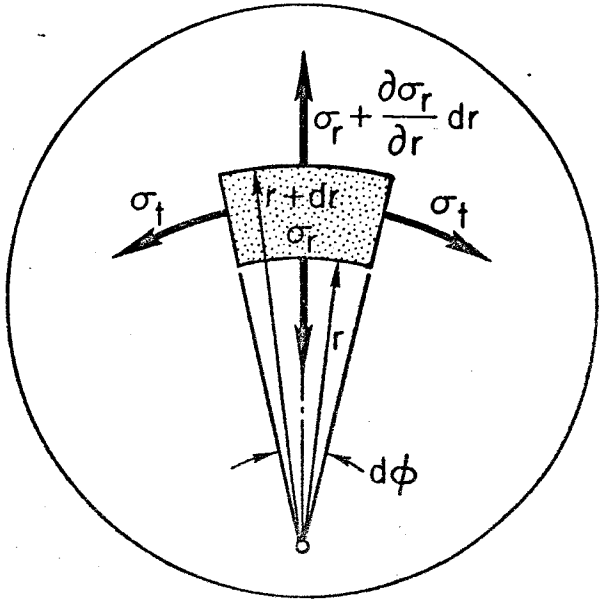

c)

DETAIL A

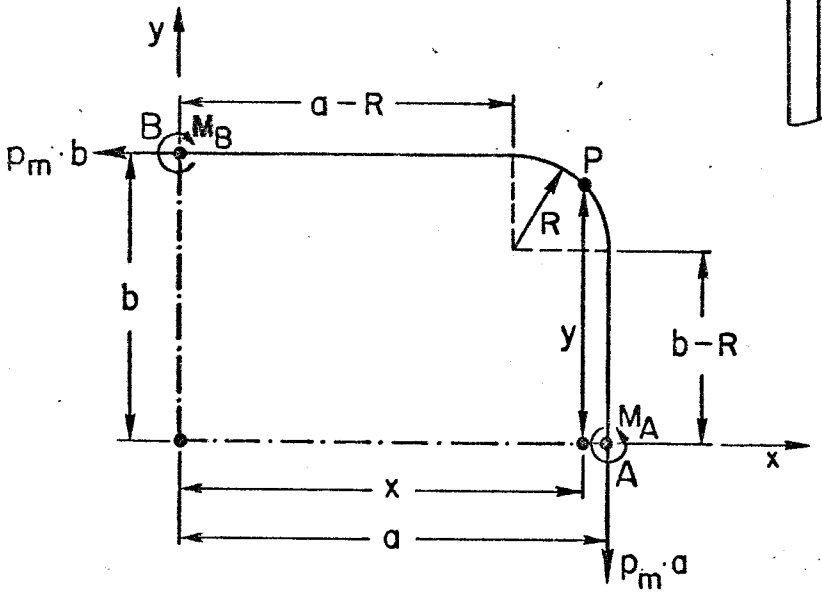

b)

D5-4

Figure 4. Two-dimensional coil geometry:
- a. Cross section through a corner
  - 1. Insulation
  - 2. Conductor
  - 3. Coolant passage
- b. Coil neutral axis
- c. Stress distribution in the insulation

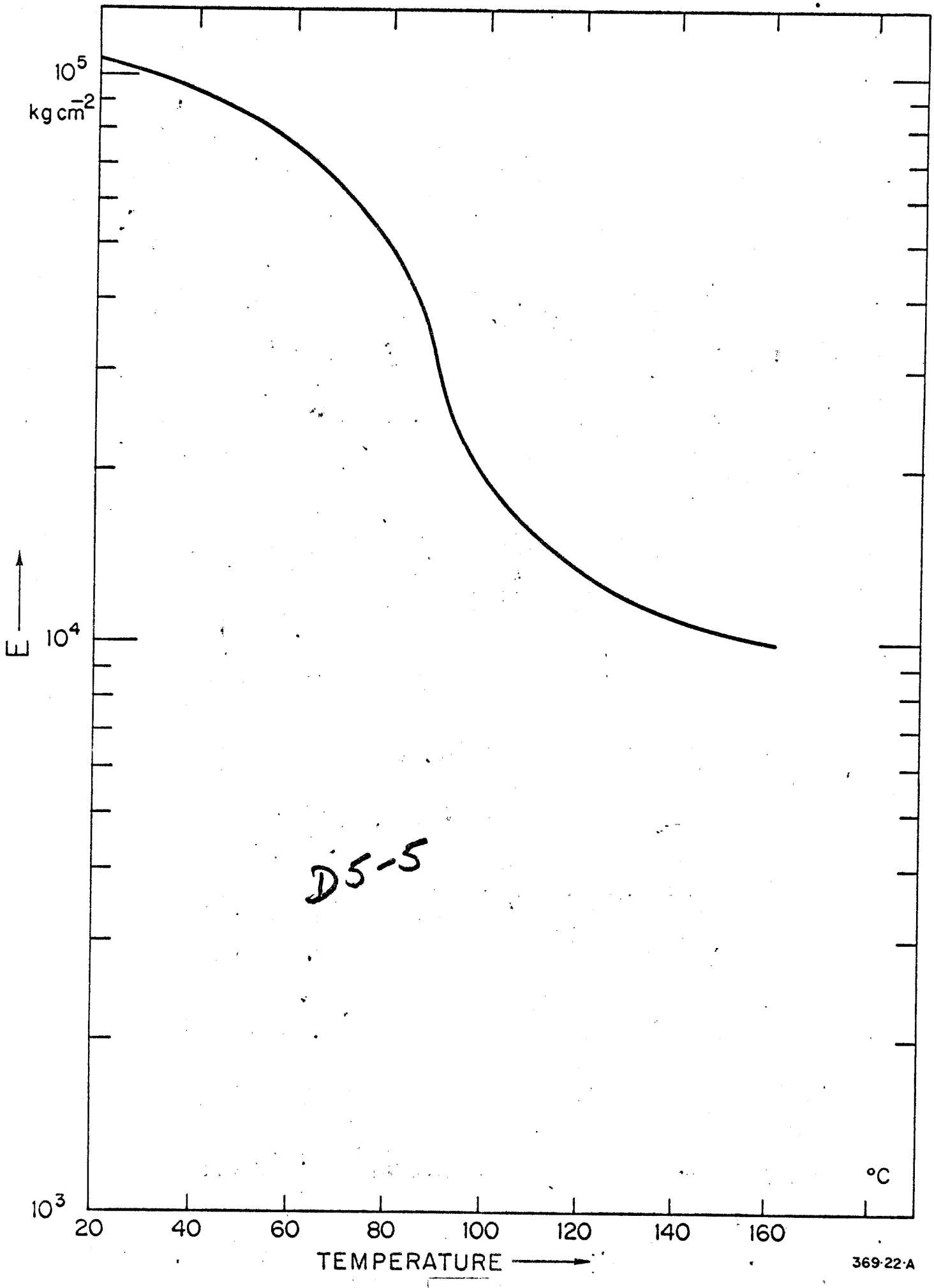
10^5
kg cm^{-2}
E
10^4
10^3
D5-5
°C
20
40
60
80
100
120
140
160
TEMPERATURE
369-22-A

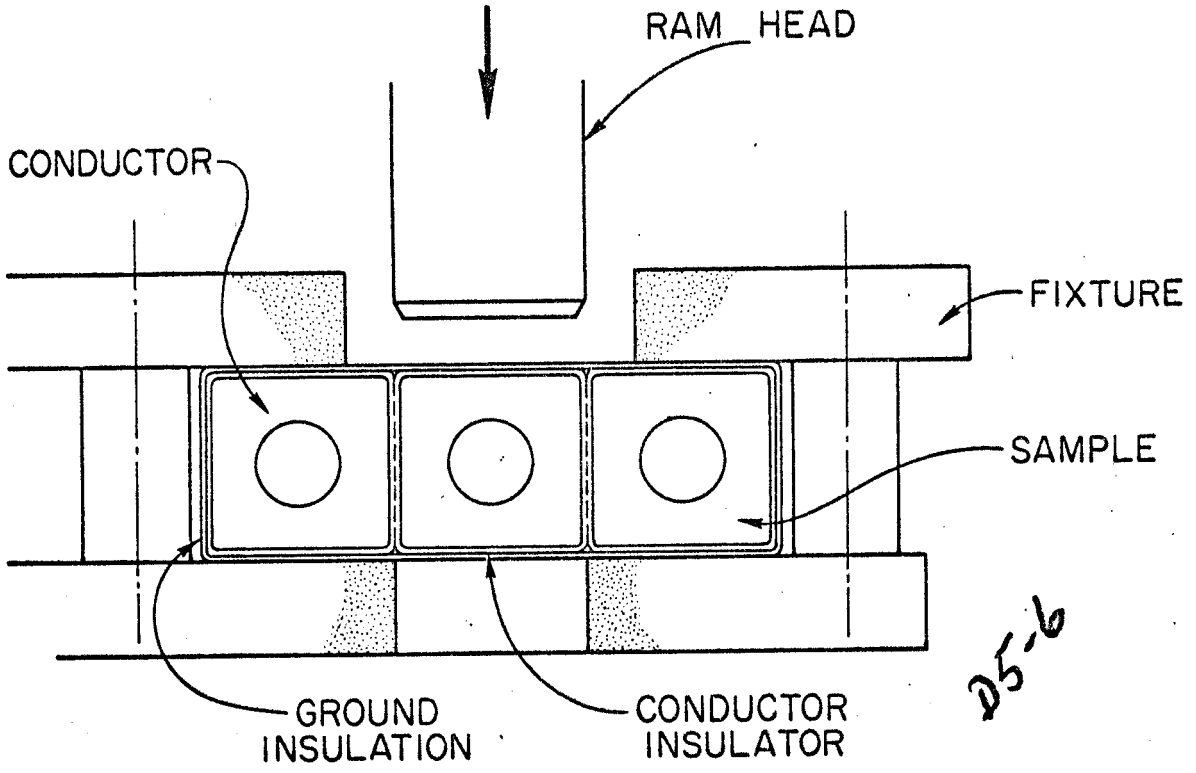
RAM HEAD
CONDUCTOR
FIXTURE
SAMPLE
GROUND INSULATION
CONDUCTOR INSULATOR
D5-6

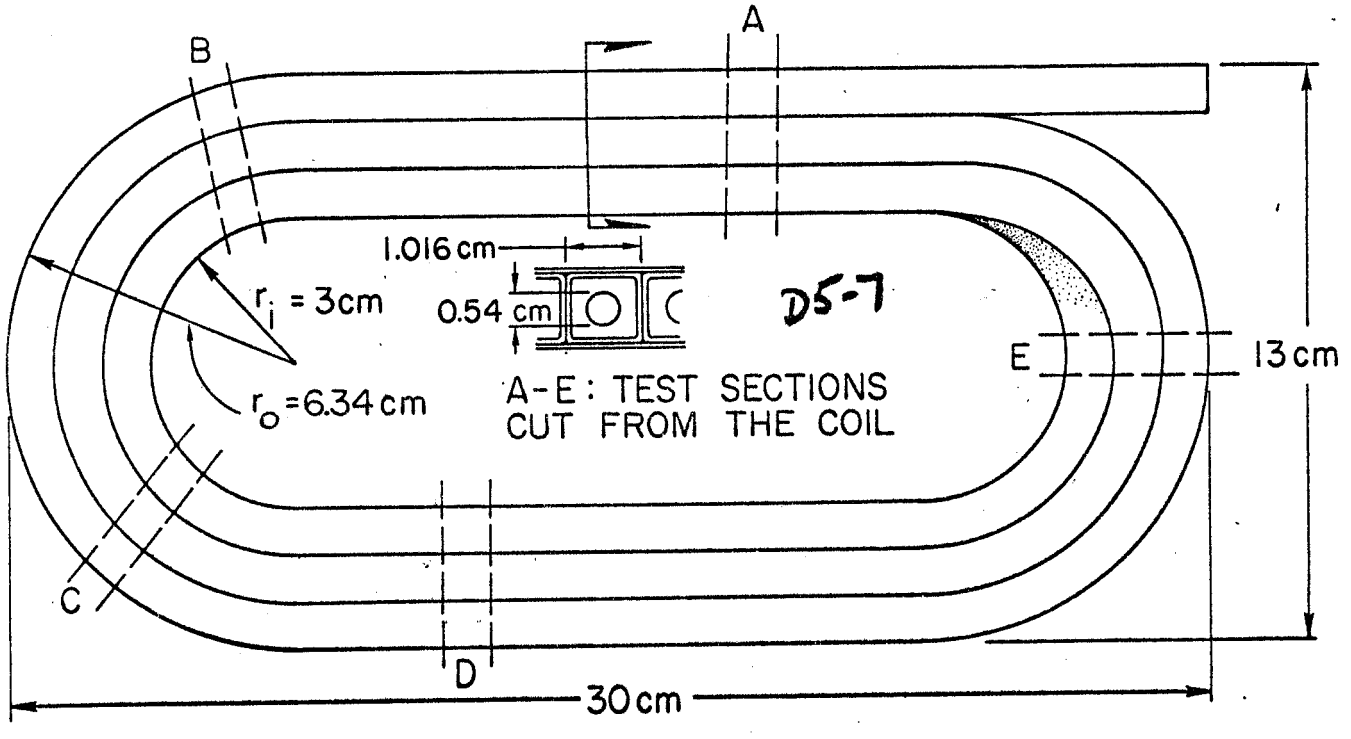
A
B
C
D
E
1.016 cm
0.54 cm
r_i = 3cm
r_o = 6.34 cm
D5-7
A-E: TEST SECTIONS CUT FROM THE COIL
13 cm
30 cm
369-1-A

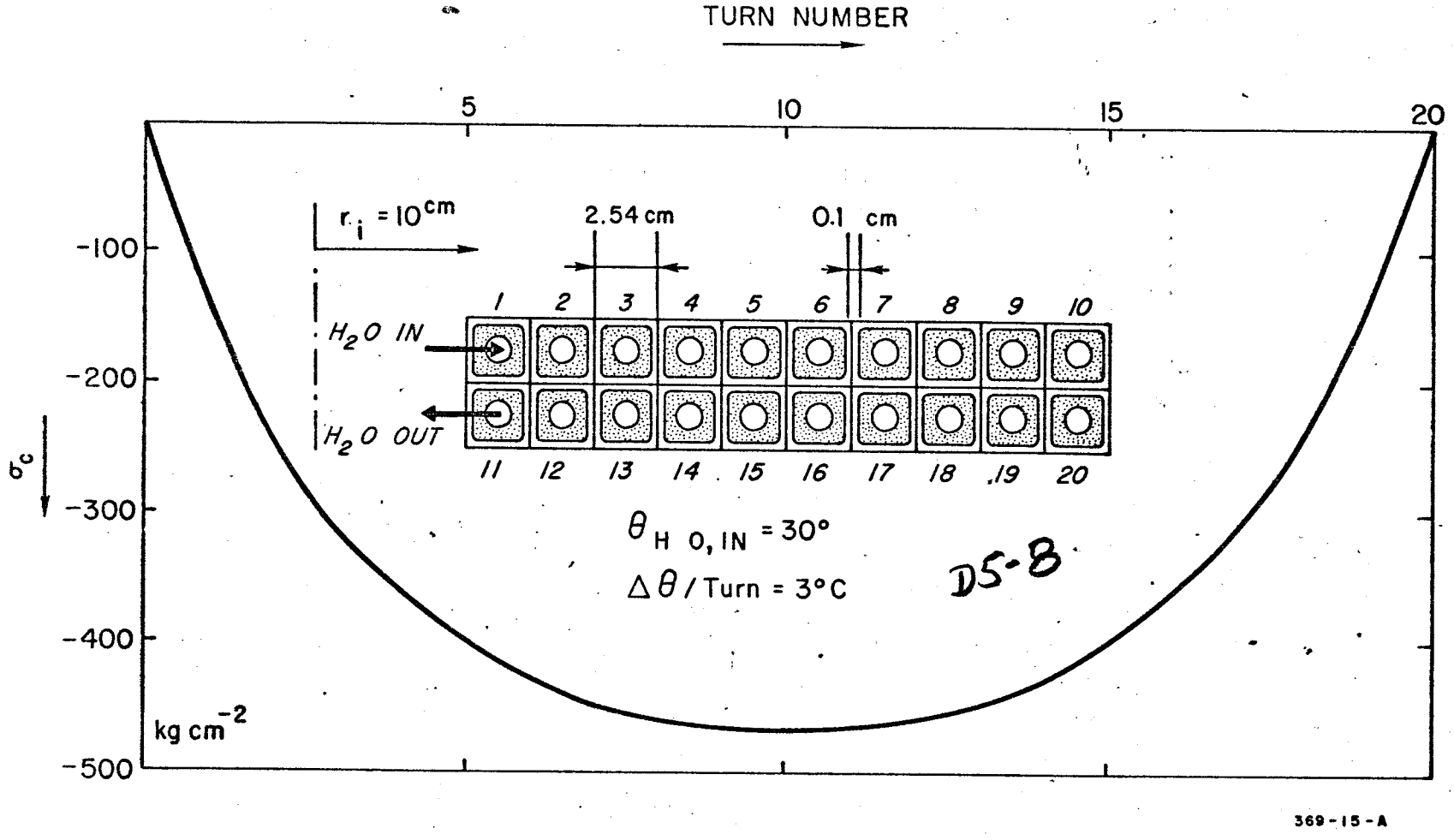
TURN NUMBER
5
10
15
20
-100
-200
-300
-400
-500
σ_c
kg cm^{-2}
r_i = 10 cm
2.54 cm
0.1 cm
1 2 3 4 5 6 7 8 9 10
H_2O IN
H_2O OUT
11 12 13 14 15 16 17 18 19 20
$\theta_{H\ O,\ IN}$ = 30°
$\Delta\theta$ / Turn = 3°C
D5-8
369-15-A

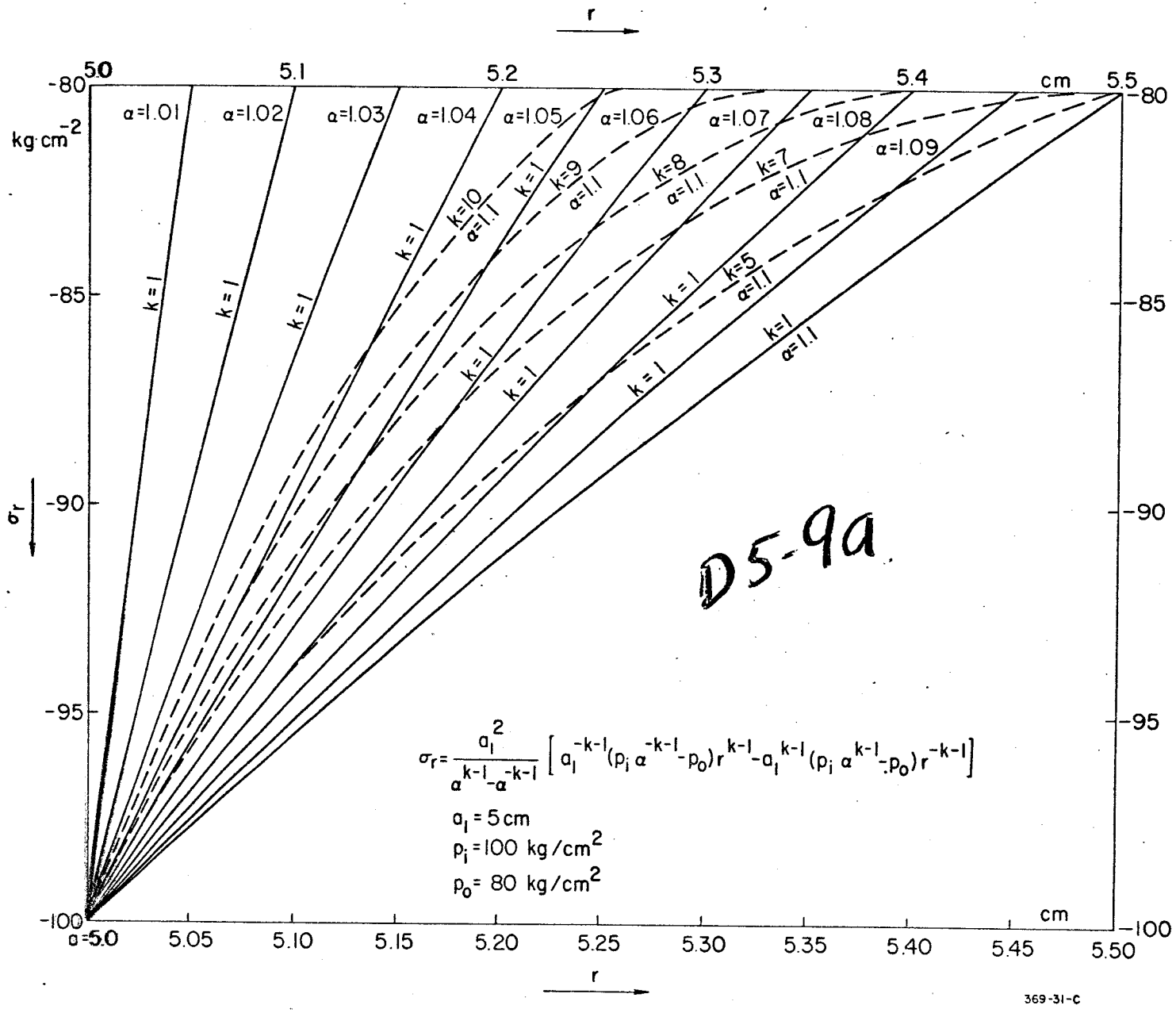
r
5.0
5.1
5.2
5.3
5.4
cm
5.5
-80
-85
-90
-95
-100
kg·cm⁻²
α=1.01
α=1.02
α=1.03
α=1.04
α=1.05
α=1.06
α=1.07
α=1.08
α=1.09
k=1
k=10 α=1.1
k=9 α=1.1
k=8 α=1.1
k=7 α=1.1
k=5 α=1.1
σr
D5-9a
$\sigma_r = \frac{a_1^2}{\alpha^{k-1} - \alpha^{-k-1}} \left[a_1^{-k-1}(p_i \alpha^{-k-1} - p_o) r^{k-1} - a_1^{k-1}(p_i \alpha^{k-1} - p_o) r^{-k-1} \right]$
$a_1 = 5\,cm$
$p_i = 100\ kg/cm^2$
$p_o = 80\ kg/cm^2$
a=5.0
5.05
5.10
5.15
5.20
5.25
5.30
5.35
5.40
5.45
5.50
cm
r
369-31-C

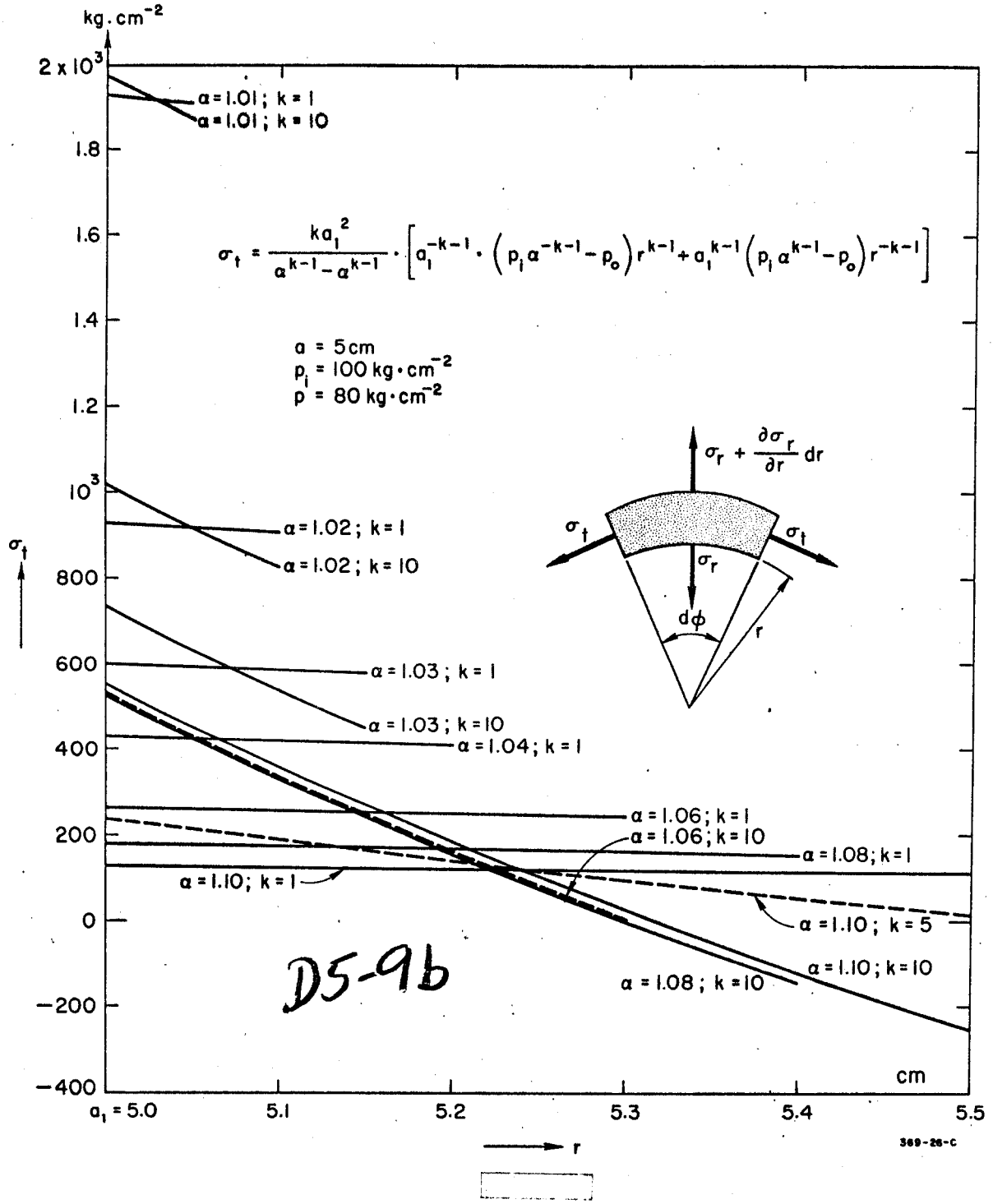
kg.cm⁻²
2 x 10³
1.8
1.6
1.4
1.2
10³
800
600
400
200
0
−200
−400
σt
α = 1.01 ; k = 1
α = 1.01 ; k = 10
σt = ka1² / (α^(k−1) − α^(k−1)) · [a1^(−k−1) · (pi α^(−k−1) − po) r^(k−1) + a1^(k−1) (pi α^(k−1) − po) r^(−k−1)]
a = 5cm
pi = 100 kg·cm⁻²
p = 80 kg·cm⁻²
σr + ∂σr/∂r dr
σt
σt
σr
dϕ
r
α = 1.02 ; k = 1
α = 1.02 ; k = 10
α = 1.03 ; k = 1
α = 1.03 ; k = 10
α = 1.04 ; k = 1
α = 1.06 ; k = 1
α = 1.06 ; k = 10
α = 1.08 ; k = 1
α = 1.10 ; k = 1
α = 1.10 ; k = 5
α = 1.10 ; k = 10
α = 1.08 ; k = 10
D5-9b
cm
a1 = 5.0
5.1
5.2
5.3
5.4
5.5
r
389-26-C

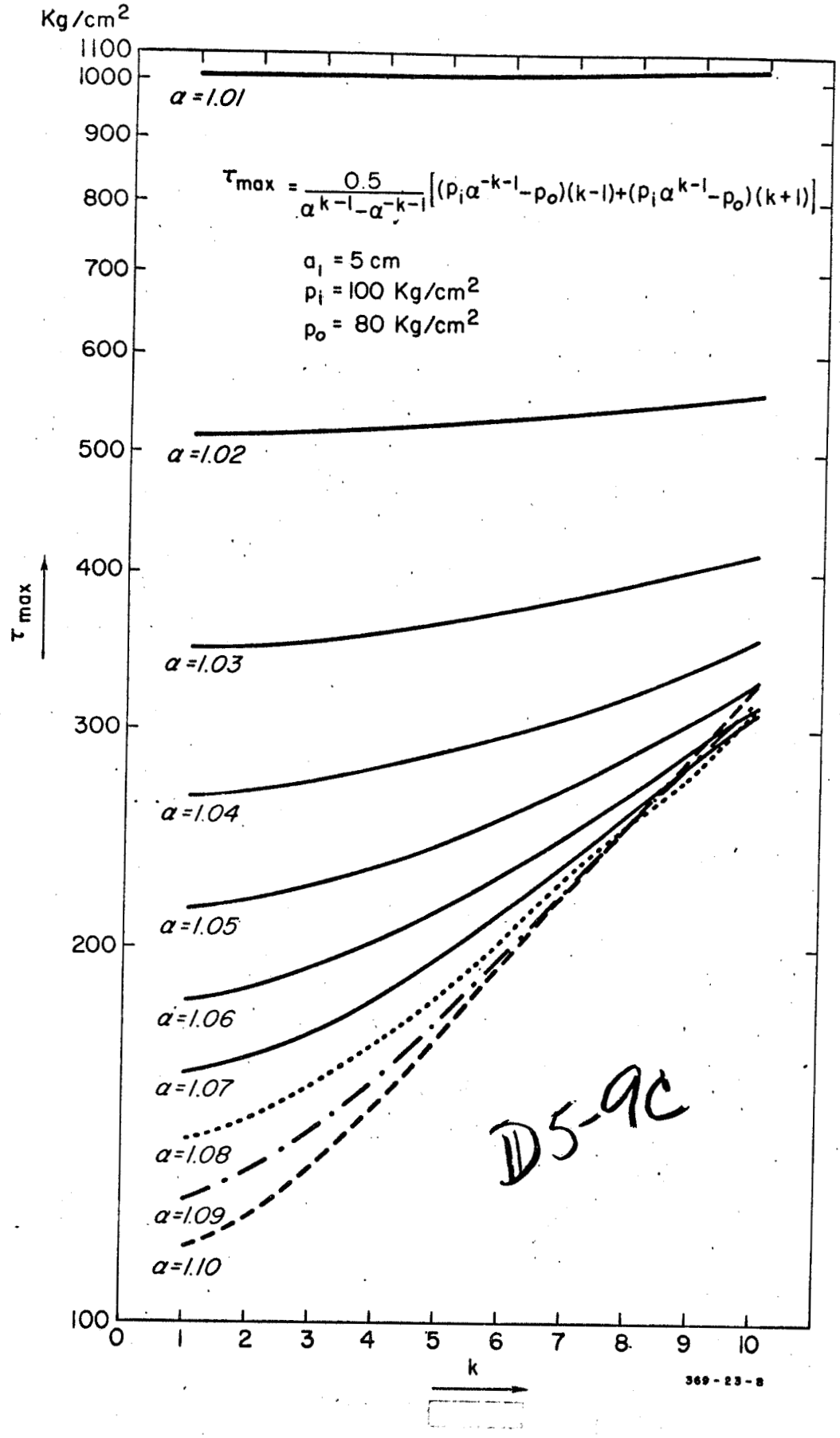
Kg/cm²
1100
1000
900
800
700
600
500
400
300
200
100
α=1.01
$\tau_{max} = \frac{0.5}{\alpha^{k-1}-\alpha^{-k-1}}\left[(p_i\alpha^{-k-1}-p_o)(k-1)+(p_i\alpha^{k-1}-p_o)(k+1)\right]$
a_1 = 5 cm
p_i = 100 Kg/cm²
p_o = 80 Kg/cm²
α=1.02
α=1.03
α=1.04
α=1.05
α=1.06
α=1.07
α=1.08
α=1.09
α=1.10
τ max
0 1 2 3 4 5 6 7 8 9 10
k
369-23-8

D5-9C

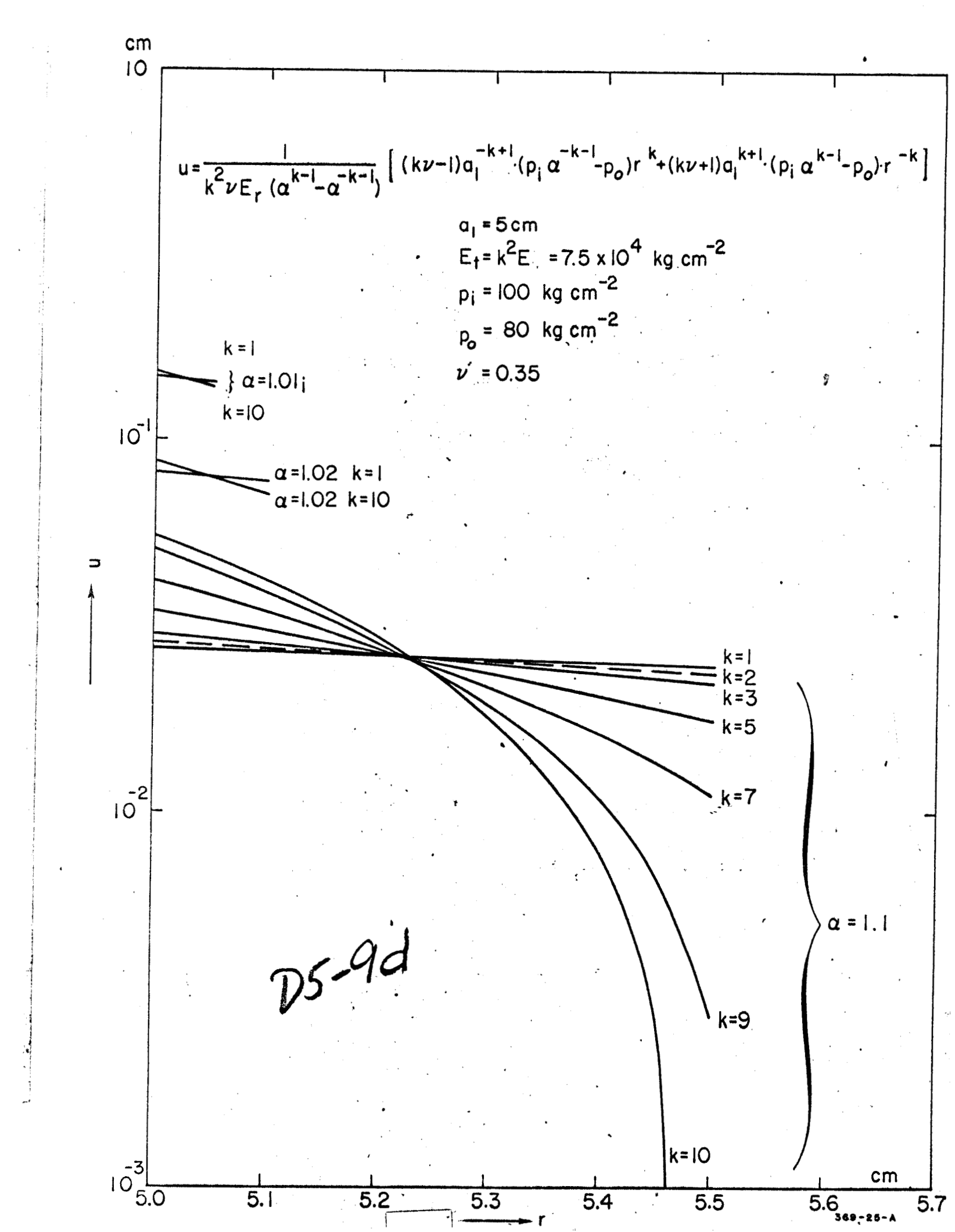
cm
10
$u = \frac{1}{k^2 \nu E_r (\alpha^{k-1} - \alpha^{-k-1})} \left[(k\nu - 1) a_1^{-k+1} \cdot (p_i \alpha^{-k-1} - p_o) r^k + (k\nu + 1) a_1^{k+1} \cdot (p_i \alpha^{k-1} - p_o) \cdot r^{-k} \right]$
$a_1 = 5$ cm
$E_t = k^2 E_r = 7.5 \times 10^4$ kg cm^{-2}
$p_i = 100$ kg cm^{-2}
$p_o = 80$ kg cm^{-2}
$\nu = 0.35$
k = 1
} α = 1.01
k = 10
10^{-1}
α = 1.02 k = 1
α = 1.02 k = 10
u
k = 1
k = 2
k = 3
k = 5
k = 7
k = 9
k = 10
α = 1.1
10^{-2}
10^{-3}
5.0
5.1
5.2
5.3
5.4
5.5
5.6
5.7
cm
r
369-25-A

D5-9d

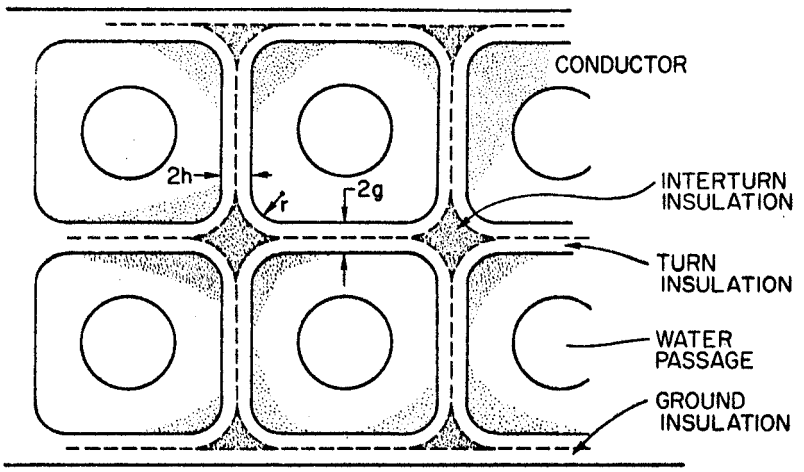

a)

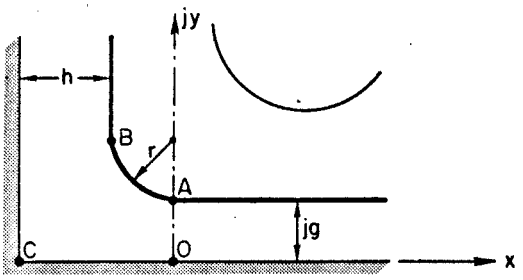

b)

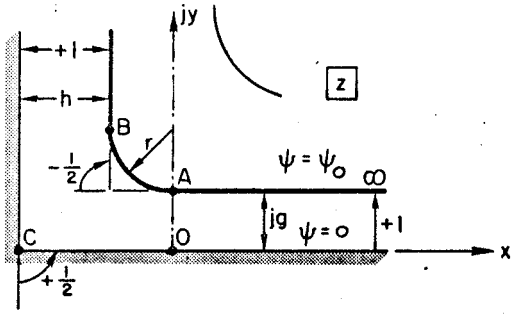

c)

D5-10

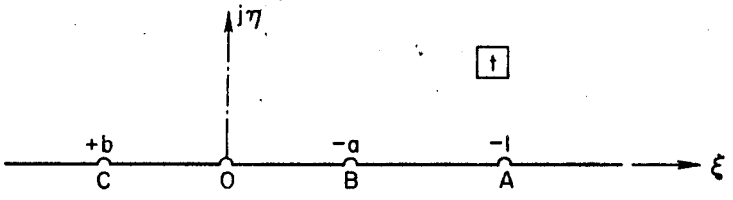

d)

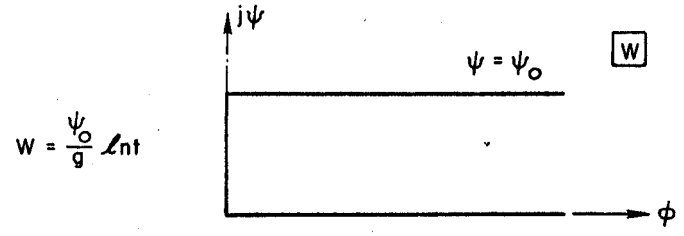

e)

369-2-8

D5-11

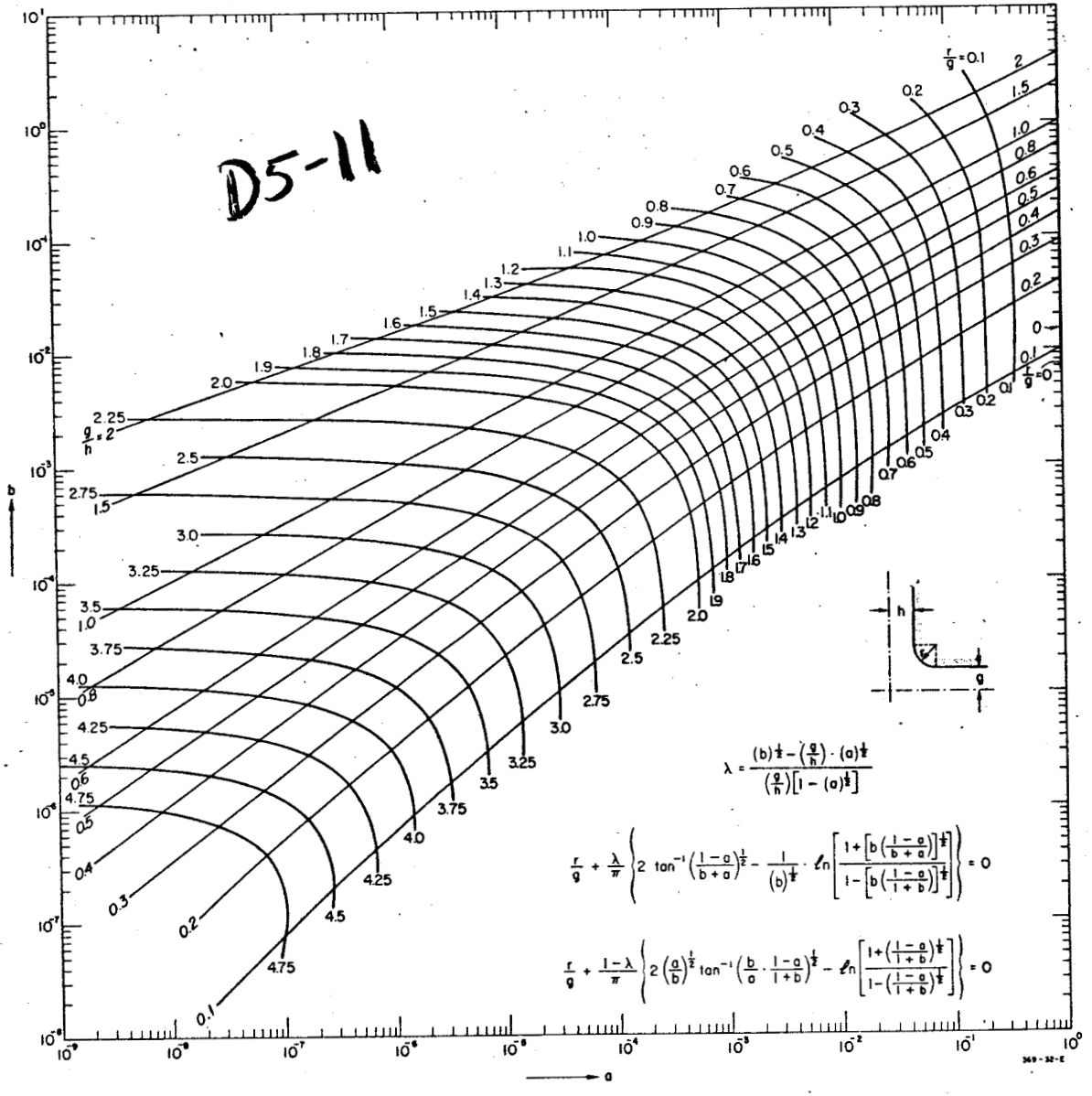
b
a
$\frac{r}{g}$=0.1
$\frac{g}{h}$=2
h
g
$\lambda = \frac{(b)^{\frac{1}{2}} - \left(\frac{a}{h}\right)\cdot(a)^{\frac{1}{2}}}{\left(\frac{a}{h}\right)\left[1-(a)^{\frac{1}{2}}\right]}$
$\frac{r}{g} + \frac{\lambda}{\pi}\left\{2\tan^{-1}\left(\frac{1-a}{b+a}\right)^{\frac{1}{2}} - \frac{1}{(b)^{\frac{1}{2}}}\cdot \ell n\left[\frac{1+\left[b\left(\frac{1-a}{b+a}\right)\right]^{\frac{1}{2}}}{1-\left[b\left(\frac{1-a}{1+b}\right)\right]^{\frac{1}{2}}}\right]\right\} = 0$
$\frac{r}{g} + \frac{1-\lambda}{\pi}\left\{2\left(\frac{a}{b}\right)^{\frac{1}{2}}\tan^{-1}\left(\frac{b}{a}\cdot\frac{1-a}{1+b}\right)^{\frac{1}{2}} - \ell n\left[\frac{1+\left(\frac{1-a}{1+b}\right)^{\frac{1}{2}}}{1-\left(\frac{1-a}{1+b}\right)^{\frac{1}{2}}}\right]\right\} = 0$

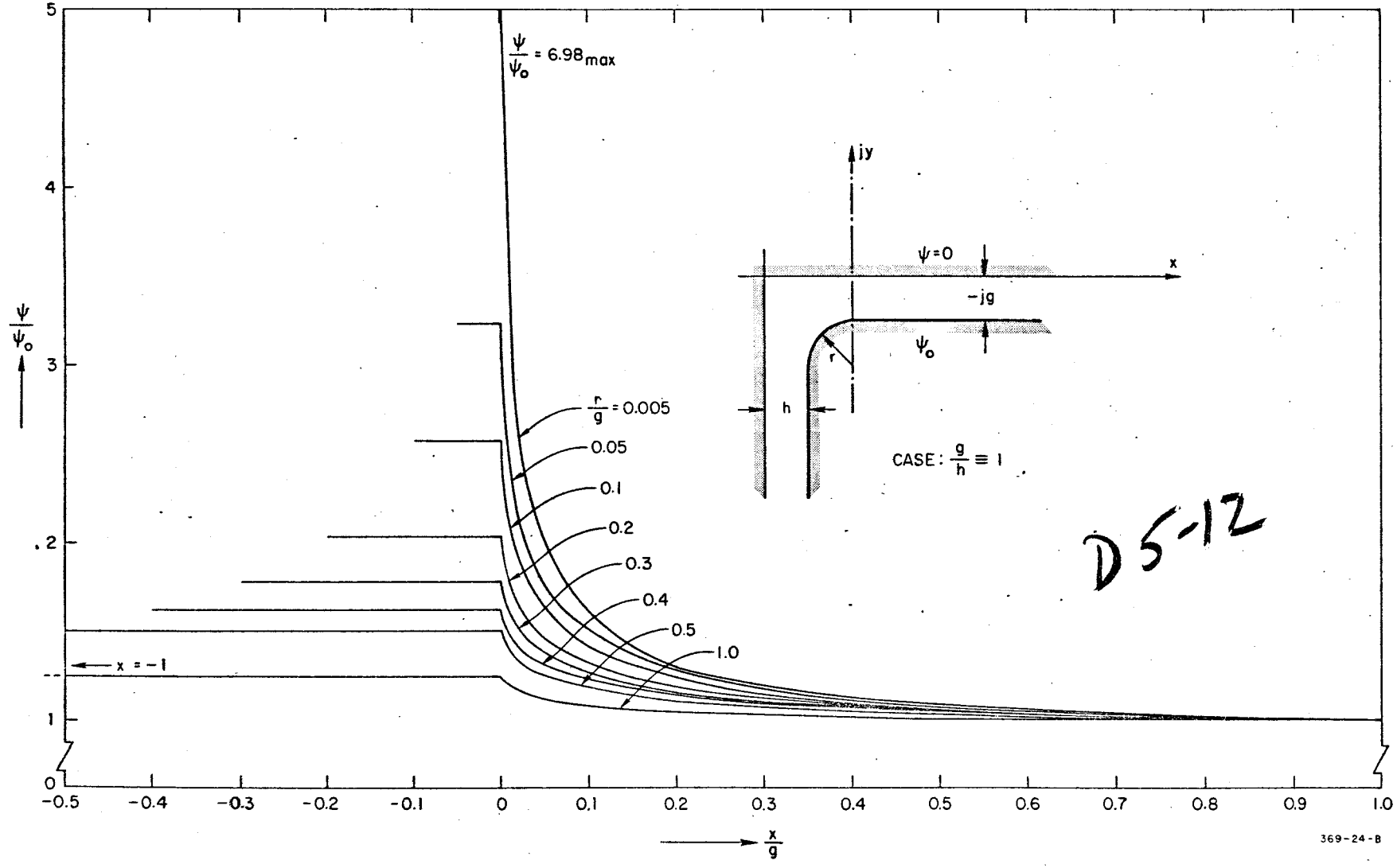
$\frac{\psi}{\psi_o} = 6.98_{max}$
jy
$\psi=0$
x
-jg
ψ_o
r
h
CASE: $\frac{g}{h} \equiv 1$
$\frac{r}{g} = 0.005$
0.05
0.1
0.2
0.3
0.4
0.5
1.0
x = -1
$\frac{\psi}{\psi_o}$
$\frac{x}{g}$
5
4
3
2
1
0
-0.5
-0.4
-0.3
-0.2
-0.1
0
0.1
0.2
0.3
0.4
0.5
0.6
0.7
0.8
0.9
1.0
369-24-B

D5-12

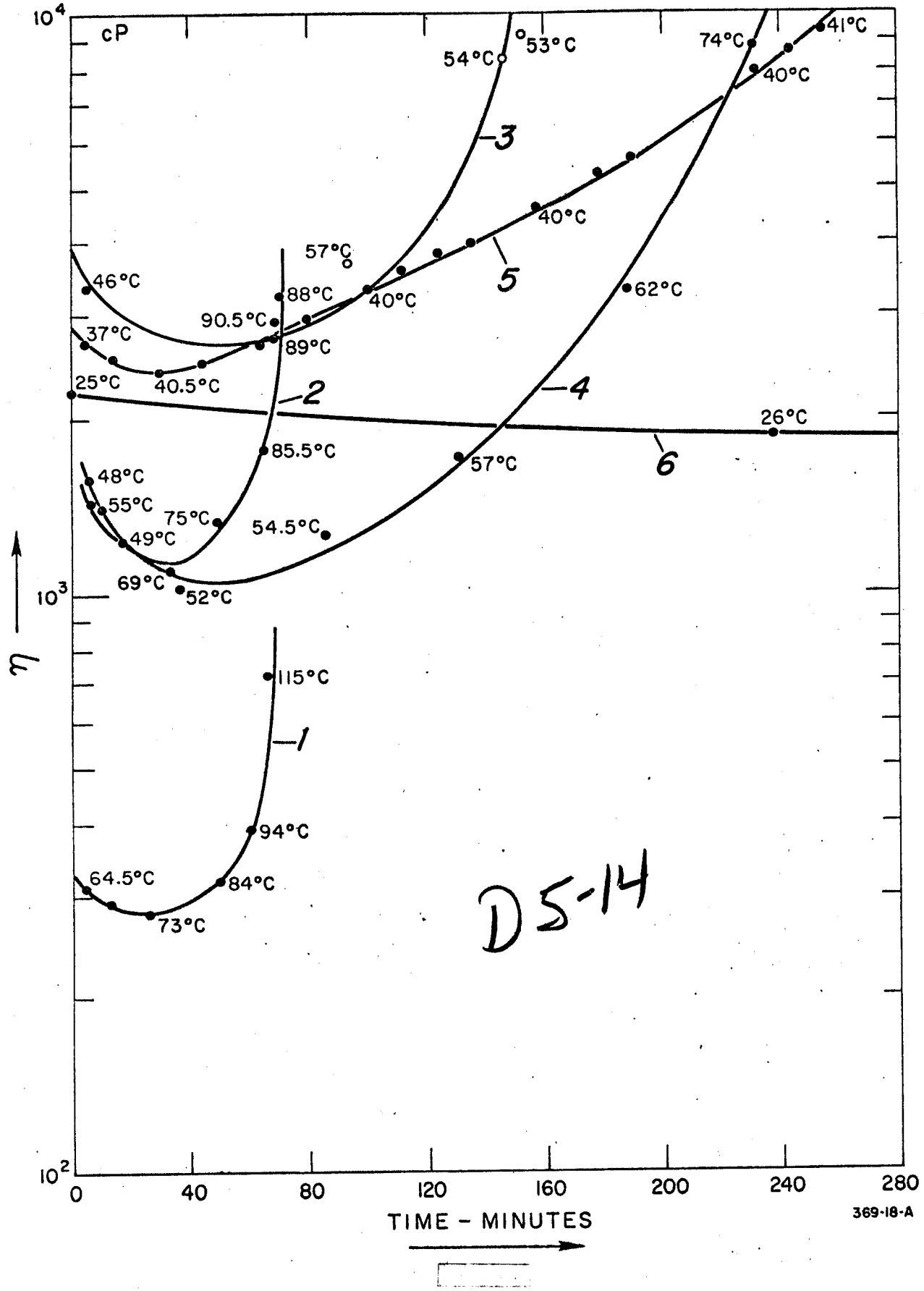
10^4
cP
54°C
53°C
74°C
41°C
40°C
3
57°C
40°C
46°C
88°C
40°C
5
62°C
90.5°C
37°C
89°C
25°C
40.5°C
2
4
26°C
85.5°C
57°C
6
48°C
55°C
75°C
54.5°C
49°C
69°C
52°C
10^3
η
115°C
1
94°C
64.5°C
84°C
73°C
10^2
0
40
80
120
160
200
240
280
TIME - MINUTES
369-18-A

D5-14

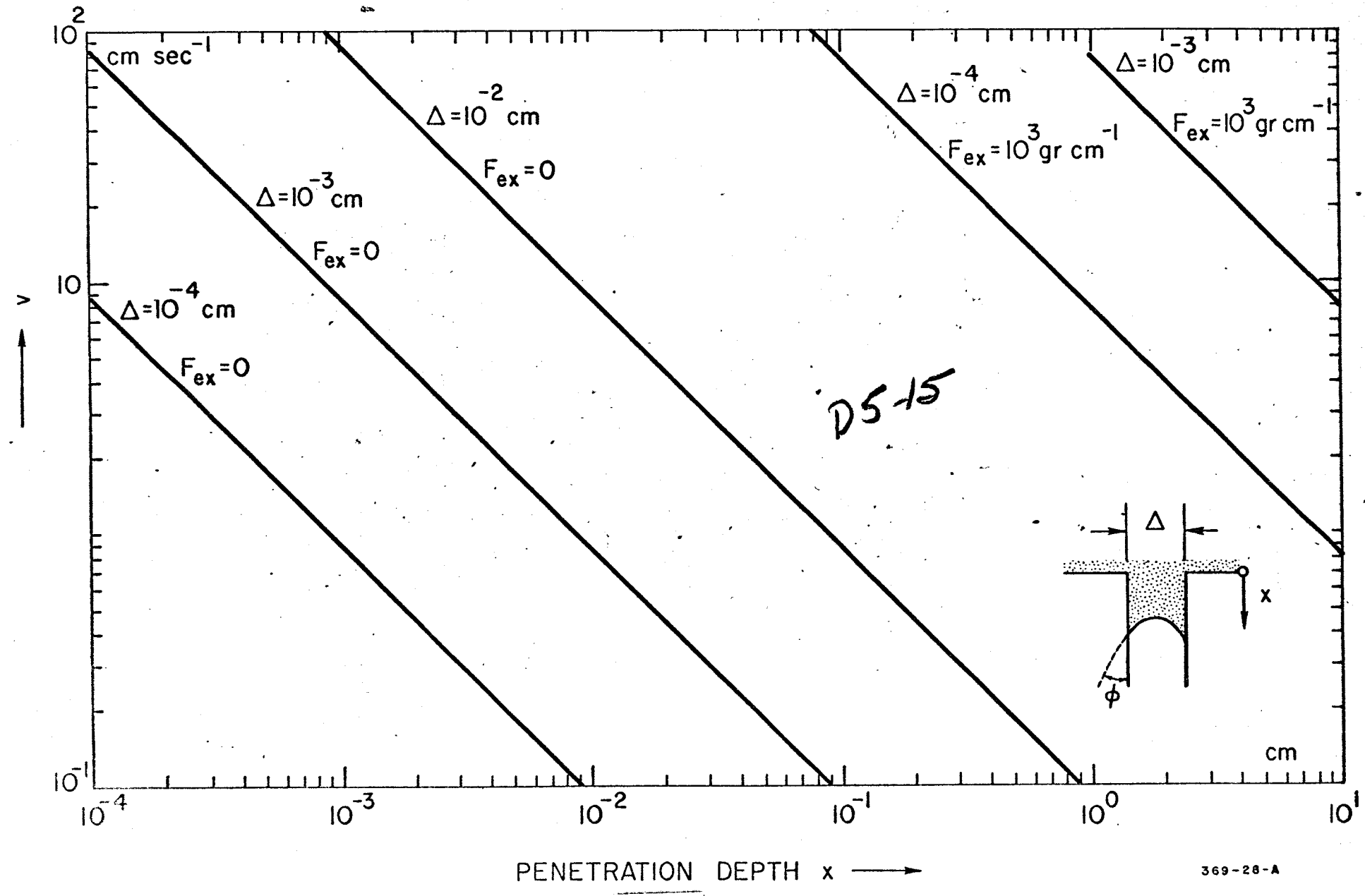
10^2
cm sec^{-1}
$\Delta = 10^{-2}$ cm
$F_{ex} = 0$
$\Delta = 10^{-3}$ cm
$F_{ex} = 0$
$\Delta = 10^{-4}$ cm
$F_{ex} = 0$
$\Delta = 10^{-4}$ cm
$F_{ex} = 10^3$ gr cm^{-1}
$\Delta = 10^{-3}$ cm
$F_{ex} = 10^3$ gr cm^{-1}
10
10^{-1}
v
10^{-4}
10^{-3}
10^{-2}
10^{-1}
10^0
10^1
PENETRATION DEPTH x
cm
Δ
x
φ
D5-15
369-28-A

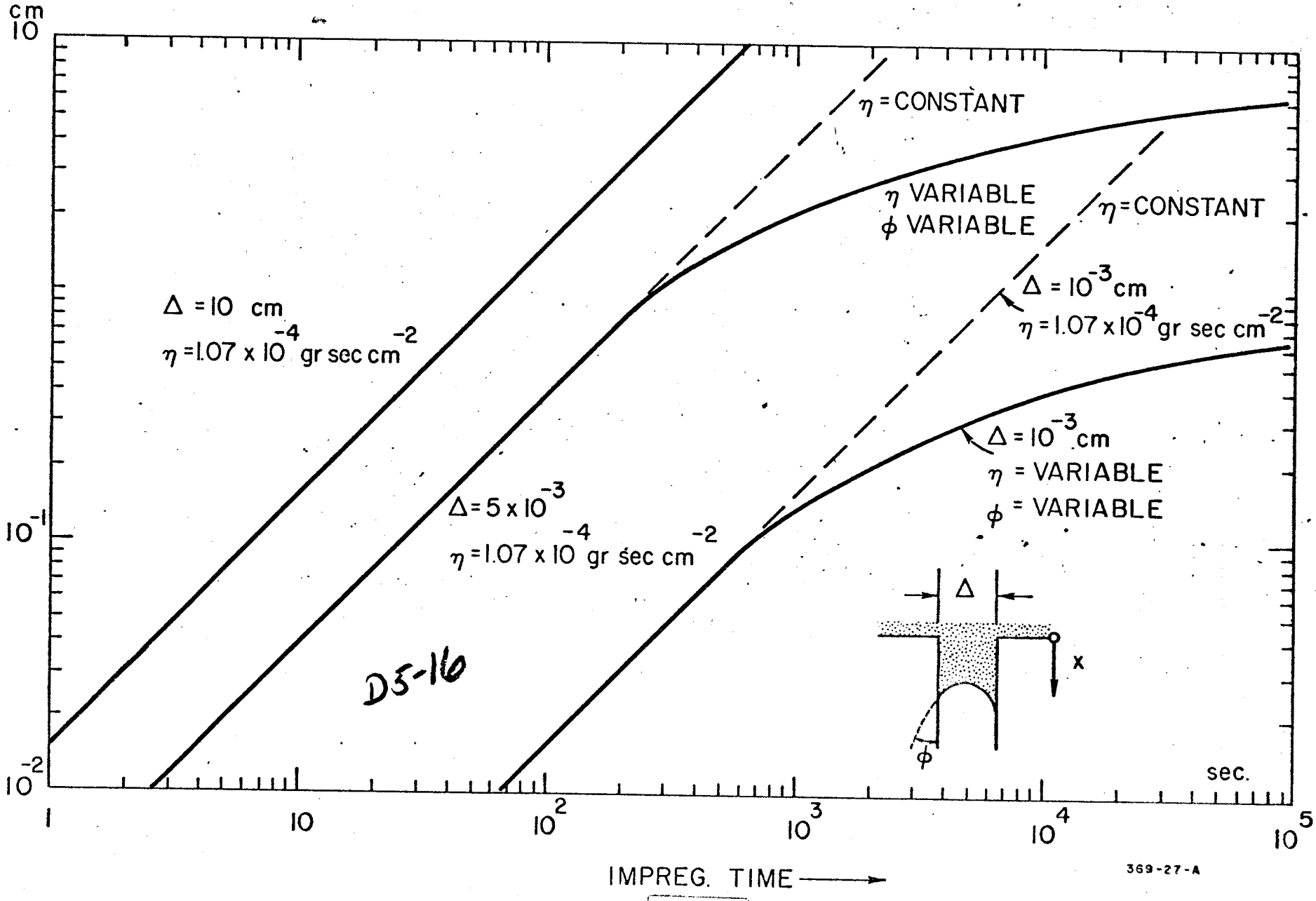
cm
10
x
10^{-1}
10^{-2}
1
10
10^2
10^3
10^4
10^5
sec.
IMPREG. TIME
η = CONSTANT
η VARIABLE
ϕ VARIABLE
η = CONSTANT
Δ = 10 cm
η = 1.07 x 10^{-4} gr sec cm^{-2}
Δ = 10^{-3} cm
η = 1.07 x 10^{-4} gr sec cm^{-2}
Δ = 5 x 10^{-3}
η = 1.07 x 10^{-4} gr sec cm^{-2}
Δ = 10^{-3} cm
η = VARIABLE
ϕ = VARIABLE
Δ
x
ϕ
D5-16
369-27-A

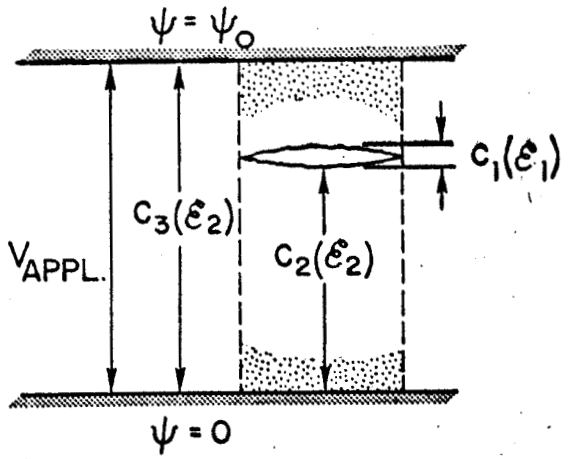
ψ = ψ0
C1(ε1)
C3(ε2)
C2(ε2)
VAPPL.
ψ = 0

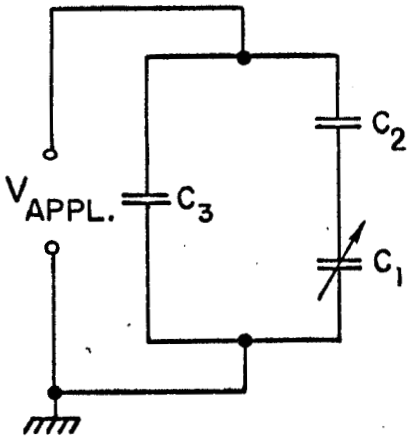
C2
VAPPL.
C3
C1

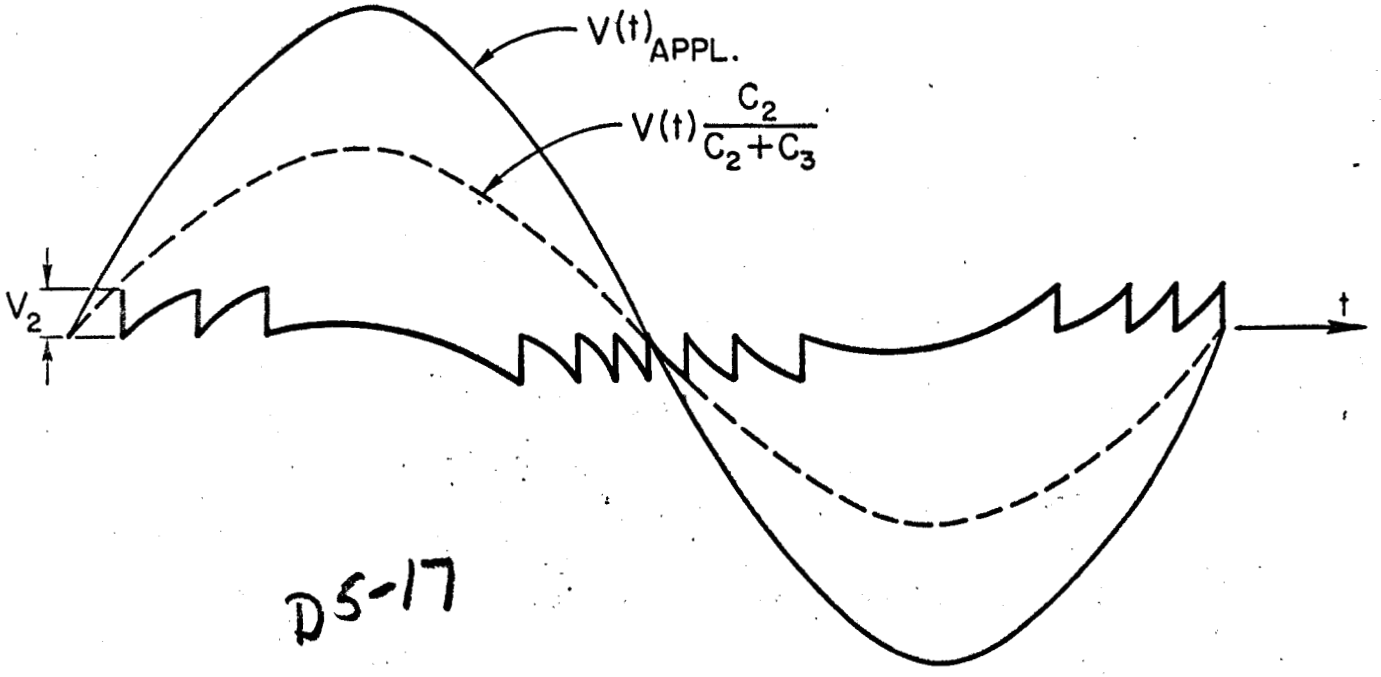
V(t)APPL.
V(t) C2/(C2+C3)
V2
t

D5-17


369-8-A

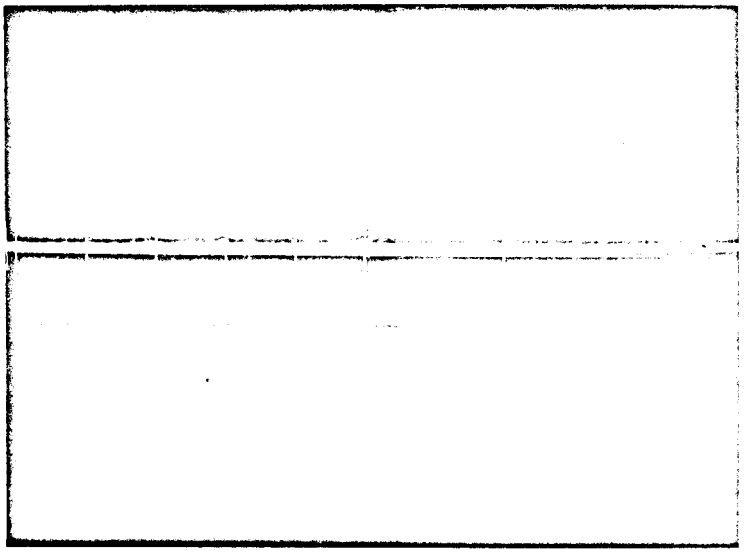

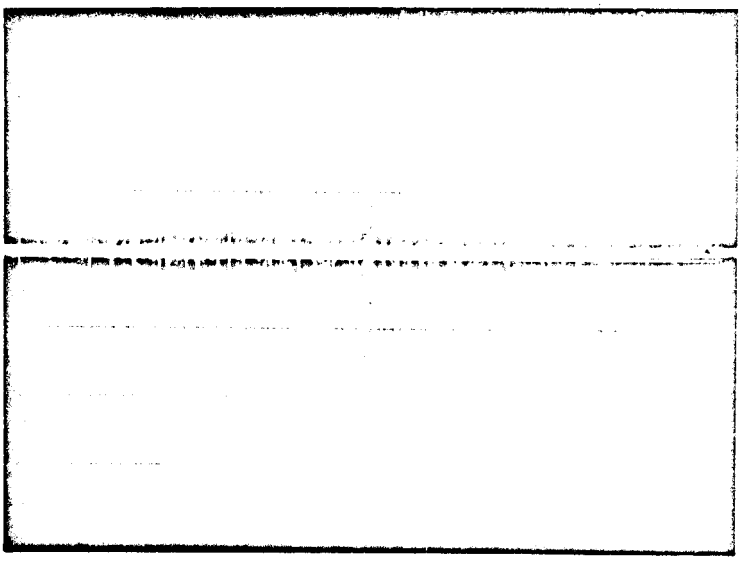

369-21-A

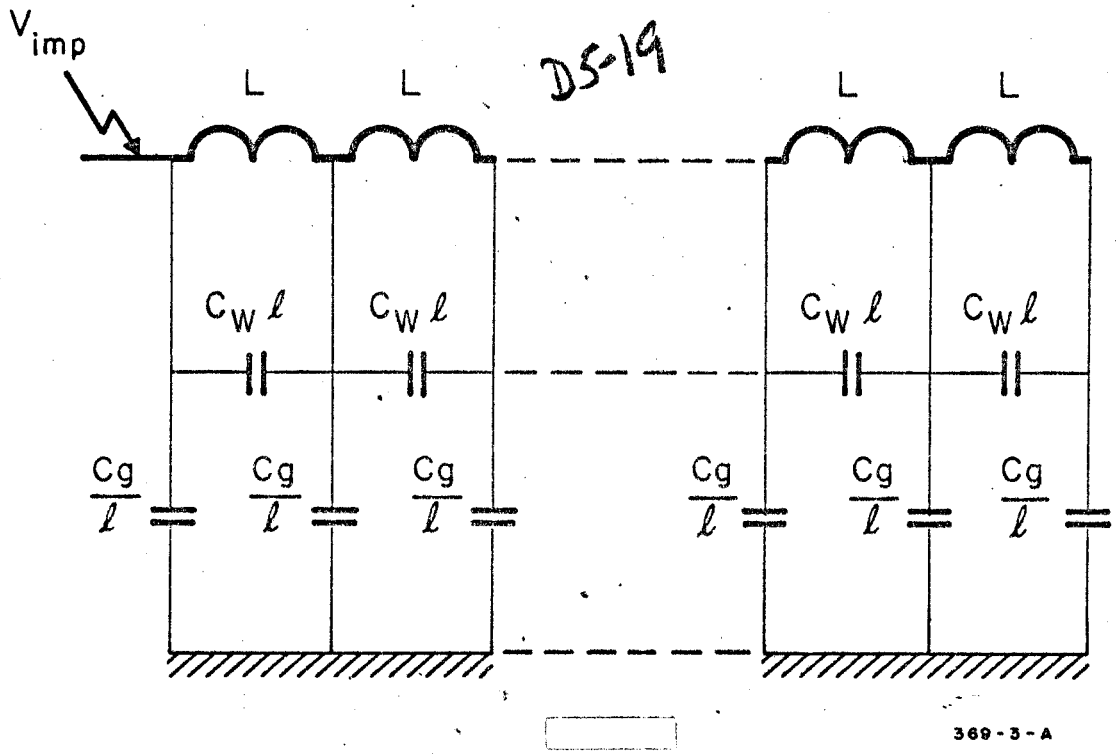
V_{imp}
L
L
L
L
$C_W \ell$
$C_W \ell$
$C_W \ell$
$C_W \ell$
$\frac{Cg}{\ell}$
$\frac{Cg}{\ell}$
$\frac{Cg}{\ell}$
$\frac{Cg}{\ell}$
$\frac{Cg}{\ell}$
$\frac{Cg}{\ell}$
369-3-A

DS-19

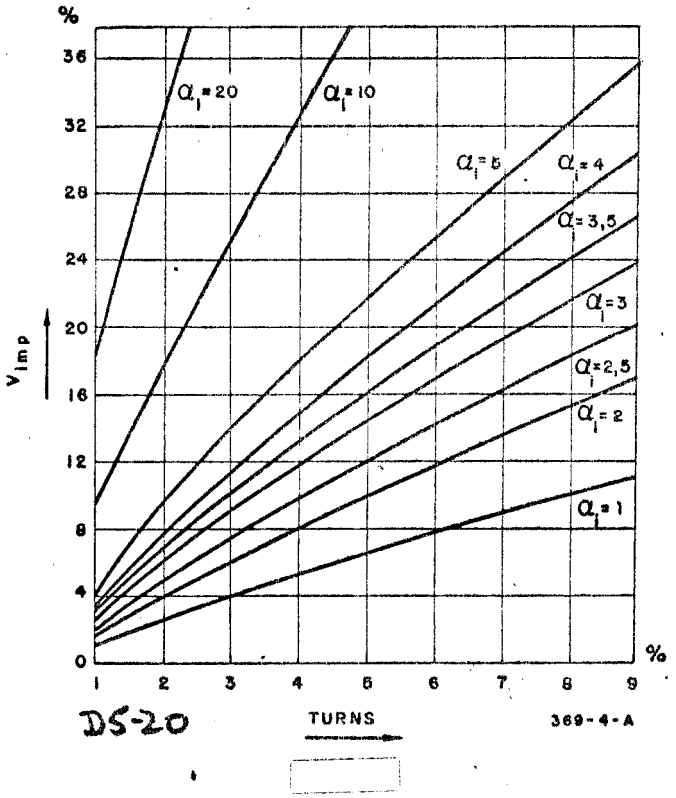
%
36
32
28
24
20
16
12
8
4
0
V_{imp}
$\alpha_i = 20$
$\alpha_i = 10$
$\alpha_i = 5$
$\alpha_i = 4$
$\alpha_i = 3,5$
$\alpha_i = 3$
$\alpha_i = 2,5$
$\alpha_i = 2$
$\alpha_i = 1$
1 2 3 4 5 6 7 8 9
%
TURNS
369-4-A

DS-20

(1)

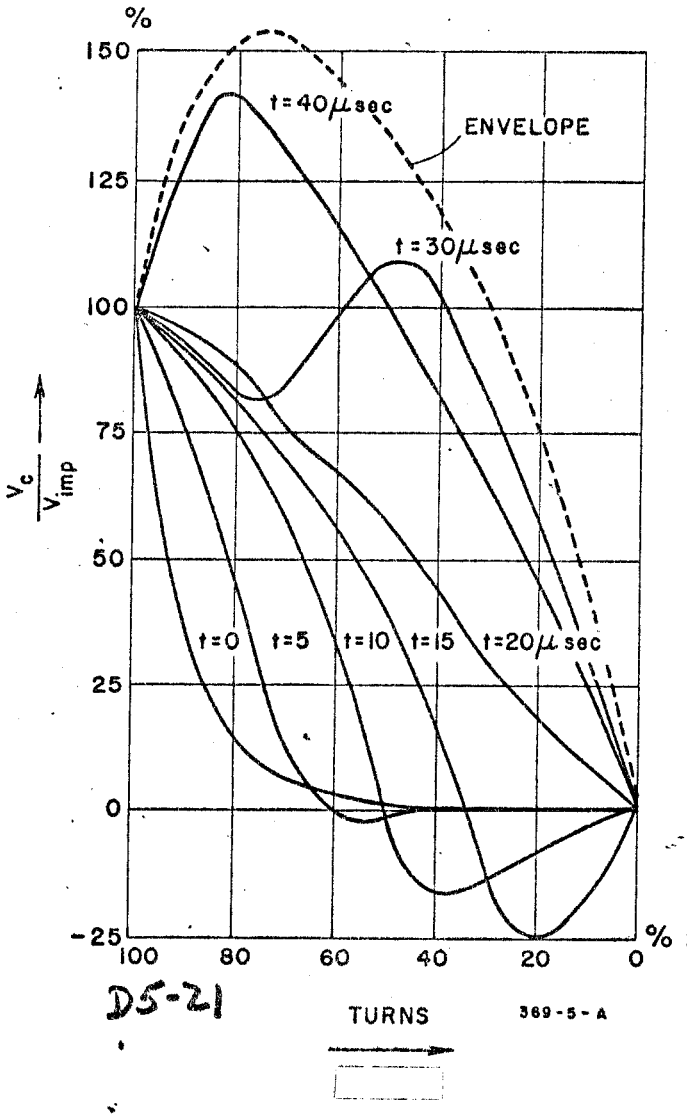
%
150
125
100
75
50
25
0
-25
t=40μsec
ENVELOPE
t=30μsec
t=0
t=5
t=10
t=15
t=20μsec
$\frac{V_c}{V_{imp}}$
100
80
60
40
20
0
%
TURNS
369-5-A

D5-21

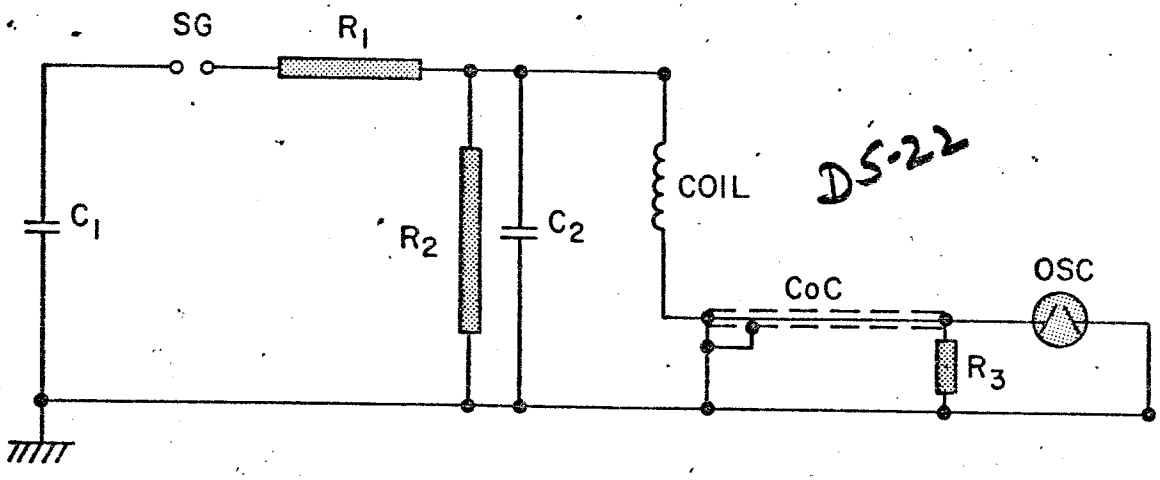

D5-22

9

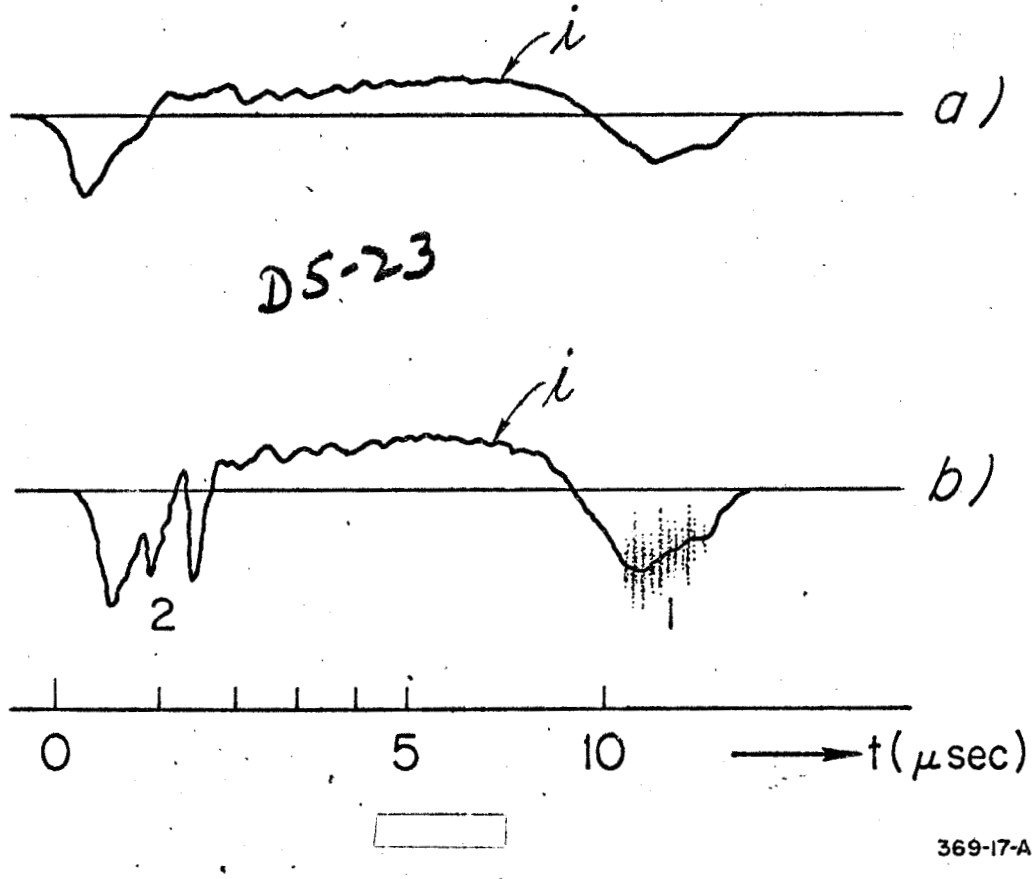

369-17-A

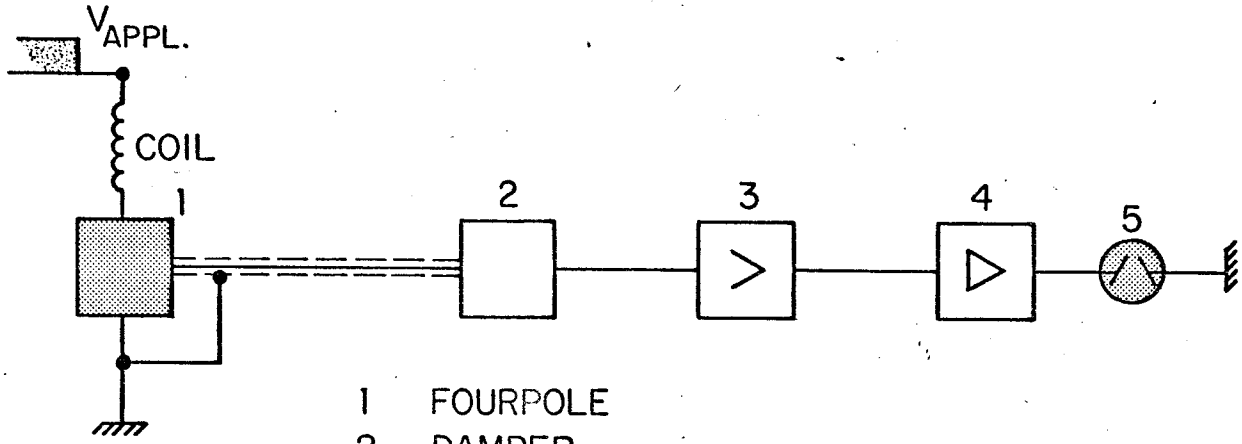

1 FOURPOLE
2 DAMPER
3 AMPLIFIER
4 COMPARATOR
5 OSCILLOSCOPE

a)

D5-24

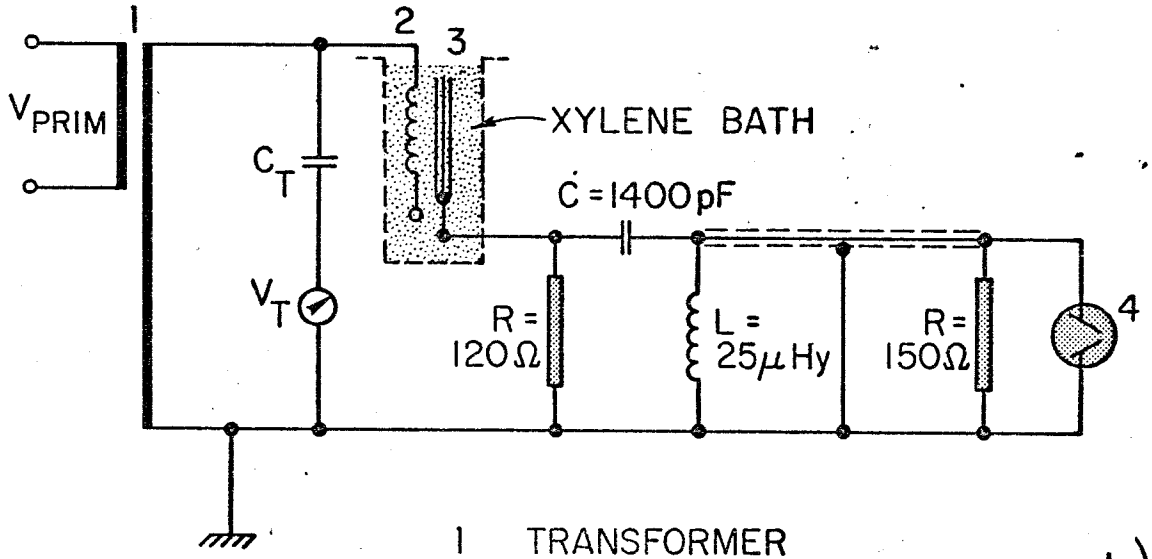

1 TRANSFORMER
2 COIL
3 PICKUP COIL
4 OSCILLOSCOPE

b)

369-7-B

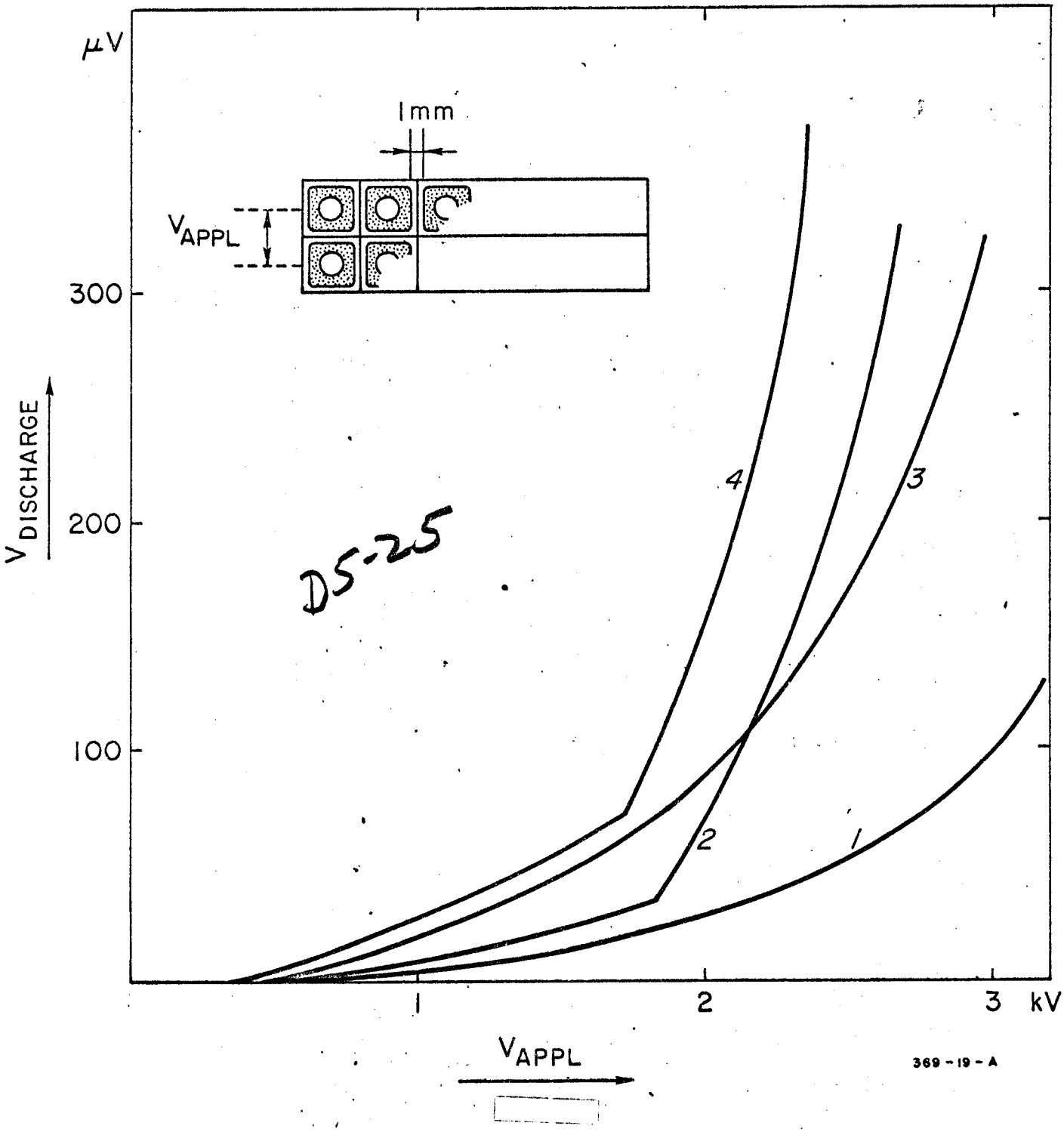
μV
1mm
V_APPL
300
200
100
V_DISCHARGE
D5-25
4
3
2
1
1
2
3 kV
V_APPL
369 - 19 - A

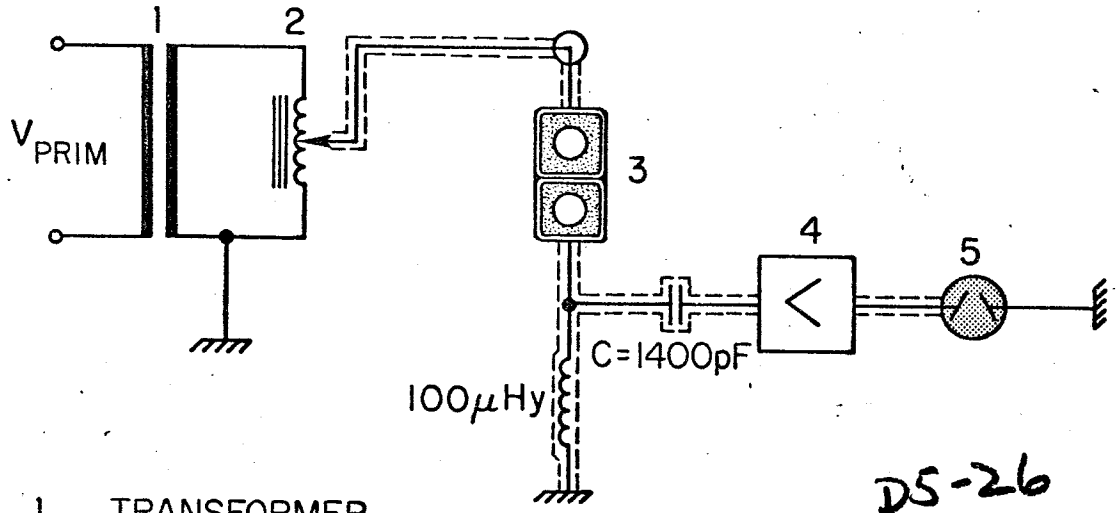

DS-26

1 TRANSFORMER
2 VARIAC
3 TEST SAMPLE OR BIFILAR WOUND COIL
4 AMPLIFIER
5 OSCILLOSCOPE

369-30-A